Contract No:

This document was prepared in conjunction with work accomplished under Contract No. 89303321CEM000080 with the U.S. Department of Energy (DOE) Office of Environmental Management (EM).

Disclaimer:

This work was prepared under an agreement with and funded by the U.S. Government. Neither the U.S. Government or its employees, nor any of its contractors, subcontractors or their employees, makes any express or implied:

1) warranty or assumes any legal liability for the accuracy, completeness, or for the use or results of such use of any information, product, or process disclosed; or
2) representation that such use or results of such use would not infringe privately owned rights; or
3) endorsement or recommendation of any specifically identified commercial product, process, or service.

Any views and opinions of authors expressed in this work do not necessarily state or reflect those of the United States Government, or its contractors, or subcontractors.

Savannah River
National Laboratory®

A U.S. DEPARTMENT OF ENERGY NATIONAL LAB • SAVANNAH RIVER SITE • AIKEN, SC • USA

Hanford Double Shell Waste Tank Corrosion Studies- Final Report FY2022

P. K. Shukla

R. E. Fuentes

J. T. Boerstler

B. J. Wiersma

<div style="text-align: center">**DISCLAIMER**</div>

Hanford Double Shell Waste Tank Corrosion Studies- Final Report FY2022

P. K. Shukla
R. E. Fuentes
J. T. Boerstler
B. J. Wiersma

July 2023

ACKNOWLEDGEMENTS

EXECUTIVE SUMMARY

For fiscal year (FY) 2022, the Savannah River National Laboratory (SRNL) focused on two experimental tasks related to Hanford Double Shell Tank (DST) chemistry and integrity. The first task focused on understanding risk of corrosion due to formation of either continuous layers or discrete patches of solids on the tanks' inner sidewalls and bottoms. The tank bottom solids contact corrosion testing focused on studying the effects of forming a dry adherent solids layer on a carbon steel substrate. Long-term exposure tests and electrochemical tests were performed to investigate the effect of drying (i.e., removing water) from the solids phase. The second task focused on corrosion of the exterior of the secondary liner. In previous years, vapor corrosion inhibitors (VCIs) were investigated as a means of mitigating corrosion of the exterior of the secondary liner. During FY22 the utilization of nitrogen was explored as a means of corrosion mitigation. The corrosion test results with nitrogen were compared with the corrosion mitigation performance of the VCIs. Conclusions for the activities that were performed in FY22 are presented below in subsections.

Underdeposit Testing

The following observations and conclusions were made from the long-term tests:

- All coupons embedded in the solids layer exhibited a similar low general corrosion rate (1-2 mpy). Additionally, the maximum pit depths measured were typically on the order of 2-5 mils. These results indicate that the environment beneath the solids is well inhibited. Given the similarity in the corrosion behavior, there is no indication that pitting increased with water content in the sludge.
- No aggressive attack was observed beneath a crevice former that was attached to the metal coupon and embedded within the solids layer. This indicates that the interstitial liquid had sufficient inhibitor to prevent crevice corrosion.
- The pits (i.e., termed micropits) measured on the coupons were much smaller in these FY22 tests than have been observed historically in uninhibited solutions. This suggests that pits may have initiated, but percolation of the inhibited interstitial liquid to the coupon surface may have repassivated the surface during the four-month test.

The following conclusions were drawn from the observations of the short-term electrochemical tests:

- The presence of the wet sludge resulted in an active shift in the negative direction of approximately $40 - 70$ mV in the open circuit potential of the carbon steel coupon as compared to the interstitial liquid . It was also noted that compression of the sludge resulted in a decrease in the open circuit potential of $10 - 20$ mV compared to that of the uncompressed sludge. The shift to more active potentials may be indicative of the initiation of localized or general corrosion beneath the solids.
- The corrosion rates measured by LPR for the interstitial liquid, the loose, wet sludge, and the compressed wet sludge were all less than 1 mpy. These rates are similar to what was observed in the long-term test and are indicative of a well inhibited environment. These corrosion rates were also corroborated by EIS measurements.
- CPP measurements in loose, wet sludge, and compressed wet sludge indicated that pitting may have initiated in the environment, but the pits were ultimately repassivated well before the completion of the test. Thus, sustainable, propagating pit are unlikely in this environment.
- Pit morphology characterization on a post-test CPP coupon indicated that the pits that formed were small. However, they tended to be broad and shallow and coalesce with neighboring pits. Thus, these pits had a morphology characteristic of carbon steel corrosion.

Secondary Liner Corrosion

The effectiveness of a nitrogen blanket for mitigating corrosion of the Hanford DSTs was investigated. The laboratory testing data showed the surface average corrosion rates are reduced by an order of magnitude in the presence of nitrogen when compared with the uninhibited conditions. These test results were compared with similar tests that were performed with a VCI. Although a complete comparison could not be made at this time due to differences in the exposure time the results seem to suggest that both effectively mitigate corrosion. A more complete comparison could be made by performing the nitrogen test for 180 days. In addition, the nitrogen and VCI-B comparison also showed that similar level of corrosion inhibition is achieved when weathered coupons were exposed to nitrogen, 100% VCI-B and 50% VCI.

Recommendations for FY23 Testing

Recommendations for follow-on work are summarized below. These recommendations will be incorporated into a proposal for FY23 activities.

Underdeposit Corrosion

➢ Investigate underdeposit corrosion under the non-porous adherent deposits with a more aggressive interstitial liquid composition (i.e., PF ≤ 1.2).
➢ Investigate the possibility of concentration cell corrosion (or cathodic polarization) beneath the sludge solids. The testing should address corrosion beneath adherent layers, the effect of concentration of the supernate above the wet, sludge layer, the effect of steel area exposed, and the effect of a temperature gradient between the supernate and the sludge solids.

Secondary Liner

➢ Investigate and determine the maximum oxygen concentration level such that corrosion is effectively mitigated. This test could be performed by varying the nitrogen blanket condition.

TABLE OF CONTENTS

LIST OF TABLES

LIST OF FIGURES

LIST OF ABBREVIATIONS

ASTM	American Society for Testing and Materials
CPP	Cyclic Potentiodynamic Polarization
DNV	Det Norske Veritas
DST	Double-Shell Tank
ER	Electrical Resistance
FY	Fiscal Year
GW	Ground Water
HLMI	Hanford Laboratory Management and Integration
LCM	Laser Confocal Microscope
LDP	Leak Detection Pit
mpy	mils per year
NDE	Non-Destructive Examination
OCP	Open Circuit Potential
PF	Pitting Factor
SCC	Stress Corrosion Cracking
SCE	Saturated Calomel Electrode
SRNL	Savannah River National Laboratory
TAPI	Tank and Pipeline Integrity
TIEP-CSG	Tank Integrity Expert Panel-Corrosion Sub-Group
VCI	Vapor Corrosion Inhibitor
VSC	Vapor Space Corrosion
WRPS	Washington River Protection Solutions

1.0 Introduction

The Hanford Site in Washington State has millions of gallons of legacy radioactive waste that is being retrieved from single-shell tanks (SSTs) and transferred to newer, double-shell tanks (DSTs) for eventual closure of SSTs. The waste will be maintained in DSTs until eventual immobilization can be performed at the Waste Treatment and Immobilization Plant (WTP), currently under construction. A detailed integrity program plan, implemented by Washington River Protection Solutions (WRPS) Tank and Pipeline Integrity (TAPI) organization, has been developed for the DSTs, which has many elements including waste chemistry control for corrosion mitigation, visual inspections and non-destructive examination (NDE) of DSTs [1].

Corrosion testing for DSTs has been guided by the Tank Integrity Expert Panel-Corrosion Sub-Group (TIEP-CSG) to provide the technical guidelines for waste chemistry control. Corrosion testing has been performed at three independent laboratories: Det Norske Veritas (DNV) Columbus, Savannah River National Laboratory (SRNL), and the 222-S facility at Hanford operated by Hanford Laboratory Management and Integration (HLMI). SRNL has focused its corrosion studies on vapor space corrosion (VSC), development of waste chemistry control limits to mitigate pitting corrosion, corrosion protection for the DST secondary liner and corrosion of the tank bottom due to contact with waste solids.

For fiscal year (FY) 2022, SRNL focused on two experimental tasks, which were continuations of activities from previous years. The first task focused on understanding the risk of corrosion due to formation of either continuous layers or discrete patches of solids on the tanks' inner sidewalls and bottoms. The second task focused on corrosion of the exterior of the secondary liner.

In FY22, the tank bottom solids contact corrosion testing focused on studying the effects of forming a dry adherent solids layer on a carbon steel substrate. Long-term exposure tests and electrochemical tests were performed to investigate the effect of drying (i.e., removing water) from the solids phase.

In previous years, vapor corrosion inhibitors (VCIs) were investigated as a means of mitigating corrosion of the exterior of the secondary liner. During FY22 the utilization of nitrogen was explored as a means of corrosion mitigation. The corrosion test results with nitrogen were compared with the corrosion mitigation performance of the VCIs.

2.0 Background

The Task Technical and Quality Assurance Plan for DST corrosion testing in FY22 included 4 activities [2]. Of the 4 activities, two were experimental studies: 1) Tank Bottom Solids Contact Corrosion Testing and 2) Secondary Liner Corrosion Testing. This report will focus on the results of these two activities. A background is provided below for these two tasks.

2.1 Underdeposit Corrosion Studies

Formation of saltcake and scale-like deposits on the wall and the bottom of several Hanford DSTs have been observed; this is based on the loose, small particulate solids in core samples taken from the tanks and post retrieval inspection of the inner surface of the primary tank of AY-102 [3]. These solids may promote underdeposit corrosion, which occurs when the liquid above the solids layer seeps in between the solids and the metal surface and creates an aggressive local environment. The objective of this task was to determine the effect of solid deposits on the corrosion risk to the tank bottom, and whether a combination

of scale, saltcake and loose solids lead to underdeposit corrosion. The potential for deposition of an adherent solids layer in this environment, and the risk of corrosion beneath the layer, was tested. The historical conditions that have existed in DST AZ-101 were selected as a representative tank for this activity. Although these conditions were utilized for initial inputs, the tests went outside these conditions in order to investigate the susceptibility, and hence the risk, for underdeposit corrosion of a tank bottom. Therefore, the results of these tests do not necessarily reflect the condition of DST AZ-101.

AZ-101 was constructed between 1970-74 and was placed into service in 1976 [4]. The tank level history is depicted in Figure 2-1. The service history for the tank may be divided into three historical intervals [4]. Between 1976-1983, the tank received waste from four sources: Evaporator Feed, Double Shell Slurry Feed, Complexed Waste and Non-Complexed Waste. A small amount of solids precipitated on the tank bottom during this period. After the waste was decanted to DST AW-102, between 1983-1989, the tank received Neutralized Current Acid Waste (Purex) from DST AY-102 and AW-101. Figure 2-2 shows that the waste temperatures approached the boiling point (~215 °F). The air circulators were used to suspend the solids, however, there was solids build-up due to settling of aluminum phases. Since that time there has been only one transfer into or out of the tank (i.e., Tank AN-106 sent a waste transfer in 2009). The temperature has been steady at approximately 145 °F. The air circulators have not been operated during this time so that the solids layer, which is 1-2 feet deep, has been undisturbed.
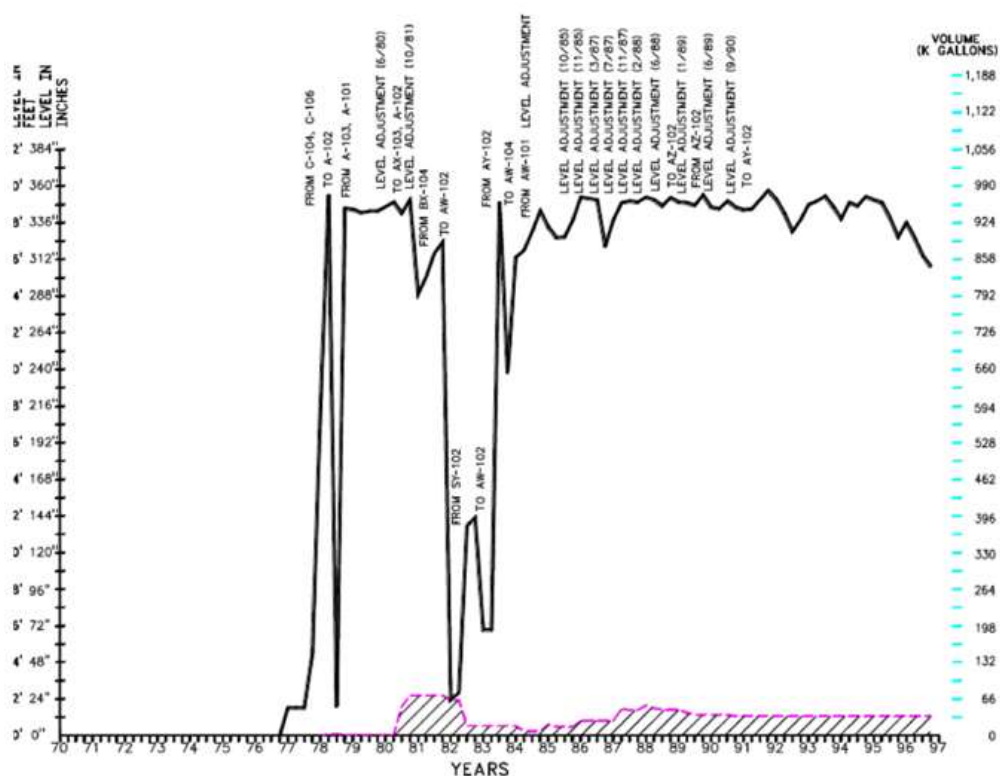
Figure 2-1: Tank AZ-101 Waste Level History from 1976 to 1988.

2
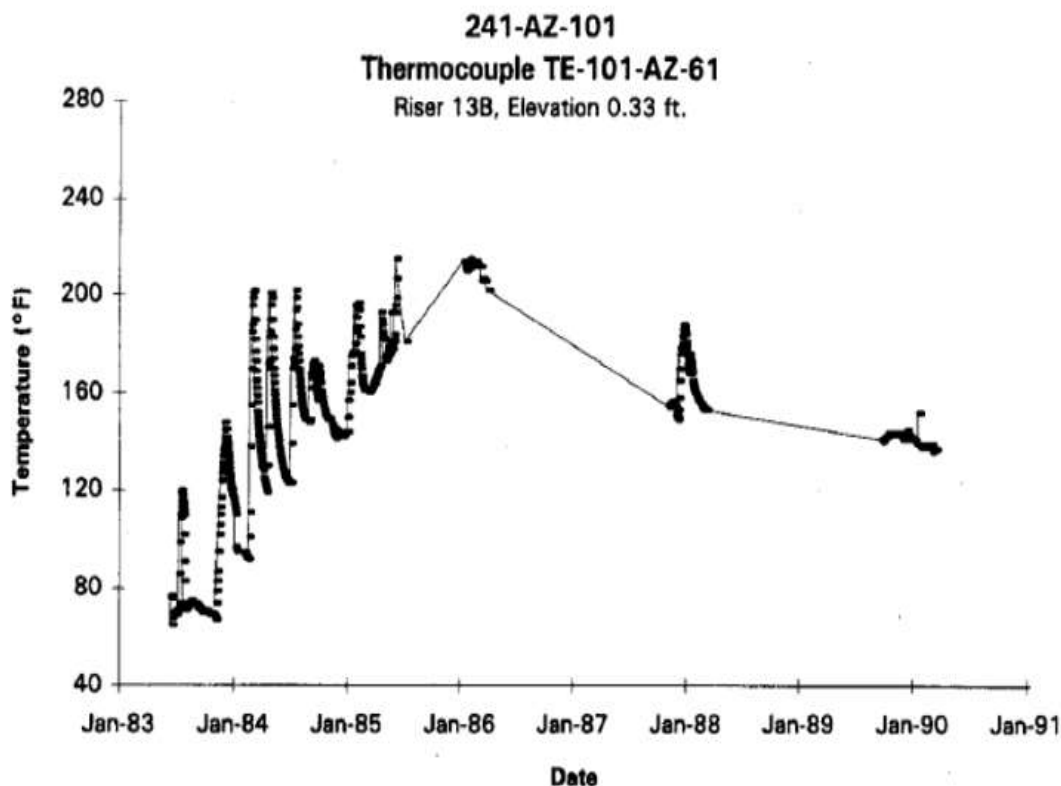
Figure 2-2: Tank AZ-101 Temperature History from 1983 to 1990.

2.2 Secondary Liner Corrosion

Each DST consists of a primary liner (inner) surrounded by a secondary (outer) liner. The secondary liner rests on a concrete foundation that contains drainage slots that will direct any leakage to a leak detection pit (LDP) [5], as shown in the schematic in Figure 2-3. Figure 2-4 shows the drainage slots that were cast into the foundation of Tanks AZ-101 and AZ-102.
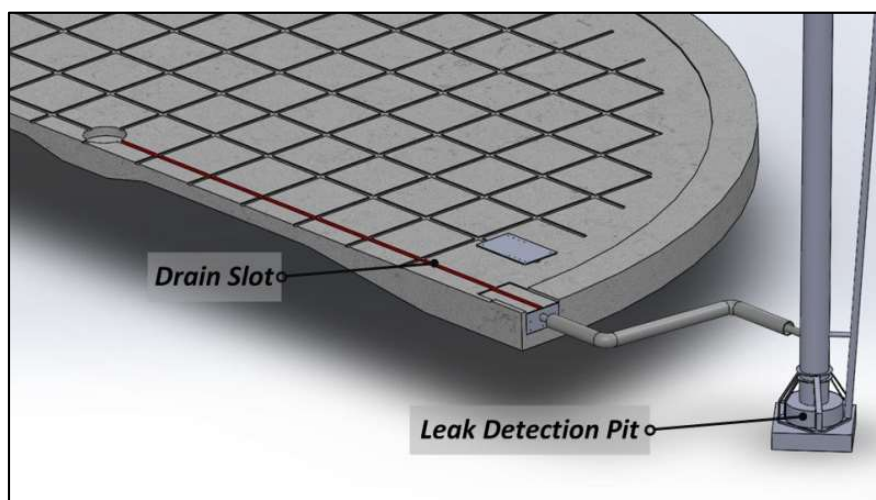
Figure 2-3: Schematic of drain slots connected to the leak detection pit (LDP).

Figure 2-4: Concrete foundation for tanks AZ-101 (foreground) and AZ-102 (background) showing the cast drainage slots.

In 2014 during ultrasonic (UT) inspection of the annulus floor in AP-102, significant material loss was observed [6]. The attack was determined to be on the exterior of the secondary liner in the gap between the liner and the concrete foundation. Since then, similar wall loss, although not as significant, has been observed in other DSTs [6]. Ultrasonic inspection is confined to the annular space between the primary and secondary tanks due to access limitations, leaving a concern that corrosion is widespread on the exterior of the secondary liner bottom plate.

Water is known to accumulate in the LDP, and by association presumably in the drainage slots, and may induce corrosion on the exterior of the secondary liner. Since the water level can vary in the drainage slots, corrosion could be caused by direct contact with the accumulated water, or when the water level is below the underside of the tank bottom, vapor space corrosion (VSC) could also occur. Accumulated water is drained through the slots into LDPs. The drained water was analyzed for its constituents, and two simulants were developed considering the chemical composition range of the accumulated water. The simulants were identified as LDP water and ground water (GW).

Testing with LDP and GW simulants for legacy carbon steel corrosion was started in FY14 with a long-term immersion experiment in which the deleterious effects of these chemistries were observed, with mass loss corrosion rates obtained of approximately 10 mils per year (mpy) [7, 8]. During FY16 testing was focused on the inhibition strategies using commercial vapor corrosion inhibitors (VCI) from Cortec Corporation to coat the samples and minimize VSC and other types of corrosion [9]. Testing continued during FY17, and it was observed that by coating the samples with VCI, the corrosion inhibition was short-lived and did not significantly reduce carbon steel corrosion [10].

In FY18, the VCI recommended dosages investigated were [11]:

- VpCI-645 + VpCI-609 solution with 10% VpCI-609 by weight of solution (100 g VpCI-609 in 1 liter) and 0.75% VpCI-645 by volume (7.5 mL/L), and
- VpCI-337 − 10% solution, i.e., 100 mL in VpCI-337 plus 900 mL of water for 1 L of the VCI solution

4

The VCIs were directly added to the groundwater solution at the start of the tests. The carbon steel coupons were immersed in the solution and, also, suspended in the vapor space of the corrosion cells. The study results indicated that both VCIs, i.e., VpCI-645 + VpCI-609, and VpCI-337, are effective in mitigating corrosion. However, one vapor space coupon in VpCI-337 environment exhibited pitting corrosion, but none in VpCI-645 + VpCI-609. This suggests that the VpCI-645 + VpCI-609 combination was slightly more effective than VpCI-337 alone in mitigating corrosion, although more tests were needed to confirm [11].

In FY19, the VCI recommended dosages investigated were [12]:

- VCI-A: VpCI-337 − 10% v/v solution in GW simulant, i.e., 100 mL in VpCI-337 plus 900 mL of GW for 1 L VCI formulation.
- VCI-B: 10% wt. VpCI-609 in GW simulant (100 g VpCI-609 in 1 liter) and 0.75% v/v VpCI-649MF (7.5 mL/L)

VCIs formulations were added after two months of exposure to the GW simulant. Three tests were conducted using VCI-A and VCI-B. It should be noted that VCI-B is a new formulation. This formulation eliminated ferric hydroxide precipitates that were observed during the FY18 tests. The first two tests were conducted using 100% recommended dosages of VCI-A and VCI-B. The third test was conducted at 10% of the recommended dosage of VCI-B. The following conclusions were made from the experimental data and results:

- The corrosion rate data indicated that 10% of the recommended dosage of VCI-B is insufficient in mitigating corrosion. This observation is consistent with a prior study which also concluded that VCIs' effectiveness vanishes at 10% of the recommended dosages for the aboveground tank bottom underside application [13].

- The data also showed that 100% recommended dosages of VCI-A and VCI-B mitigated pitting corrosion of pre-corroded coupons. Specifically, VCI-A mitigated pitting corrosion in immersed, periodically immersed and vapor space coupons, whereas VCI-B mitigated pitting corrosion in immersed and vapor space coupons. Statistical significance of corrosion rate decrease in periodically immersed coupons for 100% recommended dosage of VCI-A for some of the vapor space coupons for 100% recommended dosage of VCI-B could not be established; this may be due to coupons' surface orientation being vertical during the tests, leading to limited and uneven weathering during GW simulant only and GW simulant plus VCI exposures [12].

- After 2 months of exposure to the vapor space above the GW simulant (i.e., no VCI), the surface average corrosion rates were approximately 6.8 mpy and 2.5 mpy for the immersed and vapor space coupon, respectively. Significant pitting corrosion was also observed.

In FY20, the VCI recommended dosages investigated were [14]:

- VCI-A: VpCI-337 − 10% v/v solution in GW simulant, i.e., 100 mL in VpCI-337 plus 900 mL of GW for 1 L VCI formulation.
- VCI-B: 10% wt. VpCI-609 in GW simulant (100 g VpCI-609 in 1 L) and 0.75% v/v VpCI-649MF (7.5 mL/L)

The VCIs formulations were added after 2 months of exposure to the vapor space above the GW simulant. The tests on the pre-corroded coupons were continued for an additional 4 months. Three tests were

conducted using VCI-A and VCI-B. The first two tests were conducted using 100% recommended dosages of VCI-A and VCI-B. The third test was conducted at 50% of the recommended dosage of VCI-B. The following conclusions are made from the experimental data and results:

- Both VCIs were effective in mitigating the pitting corrosion rate for carbon steel coupons immersed in GW simulant and at the Level 2 conditions for the 100% recommended dosages. VCI-B was more effective than VCI-A in mitigating the pitting corrosion rate at Level 3 conditions.
- 50% VCI-B was also effective in mitigating the pitting corrosion rate for coupons that were immersed and at Level 1 conditions. However, a statistical analysis of the pitting corrosion rate data indicated that it was not as effective in mitigating corrosion of the coupons that were above Level 2 conditions.
- After 2 months of exposure to the vapor space above the GW simulant (i.e., no VCI), the surface average corrosion rates were approximately 5.2 mpy and 2.7 mpy for the immersed and vapor space coupon, respectively. Significant pitting corrosion was also observed.

In FY21, the two primary tests were a GW simulant only test for 6 months, which served as a control for the VCI tests, and a test with 25% of the recommended dosage of VCI-B.

The two- and six-month coupon data collected in GW only simulant indicated that aggressive corrosion continues even after the first two months of exposure. This result indicated that VCIs may effectively mitigate corrosion of the exterior of the secondary liner. In addition, the tests with 25% of the recommended VCI-B dosage showed that the inhibitor ceases to be effective at the 25% level. Based on previous results from testing in FY19 and FY20, the threshold minimum dosage for VCI-B is between 25 and 50% of the recommended dosage. In practice, if the concentration of VCI-B decreases below 50%, it is likely that replenishment of the VCI would be necessary.

3.0 Task Description and Activities

The tasks and activities that were performed during FY22 are listed and described in the sections below.

3.1 Task 1: Completion of FY21 report

Task 1 was the completion of the FY21 report. The report was completed and issued in September 2022[15]. It included work on Underdeposit Corrosion Studies and Secondary Liner corrosion testing using VCI formulations.

3.2 Task 2: New Chemistry Control Limits Implementation and Technical Support

SRNL provided technical advisory services in this support activity. SRNL participated in bi-weekly telecons, which involved preparing updated reports and making oral presentations to the TIEP-CSG. SRNL personnel also participated in an in-person annual meeting in Columbus, OH during September 2022. Reports or notes on these meetings are kept by the Chairman of the Tank Integrity Expert Panel. All meetings were virtual. No further description of these events will be presented in this report.

3.3 Task 3: Underdeposit Corrosion Beneath Tank Bottom Solids

The results from the FY21 study indicated that micropits form beneath adherent solid deposits [15]. For this task then, the focus was put into the formation of adherent, low porosity deposits from AZ-101 including a supernate simulant and an insoluble solid component. Both long-term exposure and

electrochemical tests under compression were performed to further investigate the attack beneath the adherent solids.

3.4 Task 4: Secondary Liner Corrosion Testing

Previous secondary liner corrosion experiments focused on the effectiveness of VCIs to mitigate corrosion of carbon steel immersed in a GW solution and in the vapor phase above the solution. Tests in FY22 will examined the effectiveness of de-aerating the system for corrosion mitigation in the solution and in the vapor phase. Using the same set-up that was utilized for the VCI tests, a nitrogen blanket was applied to the vessel. The tests assessed the performance of pre-corroded and polished sample in the de-aerated atmosphere.

4.0 Experimental Procedure

4.1 Materials for Testing

The material used for all corrosion testing was carbon steel selected from AAR TC-128 Rail Car Steel. This steel was selected for testing since it approximates the chemistry and microstructure of American Society for Testing and Materials (ASTM) A515, Grade 60 carbon steel, the steel from which the DSTs in AY-Farm and AZ-Farm were fabricated [16]. The chemical composition of the steel is shown in Table 4-1.

Table 4-1: Chemical Composition of AAR TC-128 Rail Car Steel

	C	Mn	P	S	Si	Fe
Specification (wt.%)	0.24 (max.)	0.9 (max.)	0.035 (max.)	0.04 (max.)	0.13 to 0.33	Balance
Measured (wt.%)	0.212	1.029	0.012	0.013	0.061	Balance

4.2 Underdeposit Corrosion Testing

4.2.1 Preparation of AZ-101 Interstitial Liquid Simulant

The most recent sample of the interstitial liquid was obtained in 1999 as shown in Table 4-2 [17]. The pitting factor (PF) for this composition is on the order of 4.6. Best Basis Inventory compositions are calculated by WRPS to project the anticipated chemistry of the waste over time. The projected chemistry of the interstitial liquid in 2018 is also shown in Table 4-2. The pitting factor had decreased to a value slightly below 2. The modified AZ-101 simulant composition utilized the original sample results as well as the concept that the solution chemistry may become more aggressive (i.e., PF on the order of 2). The sample chemistry was modified by adjusting the hydroxide ion concentration such that the pitting factor is less than 2 [18]. OLI™ was utilized to adjust values for aluminum, sulfate, carbonate, and fluoride in order to minimize precipitation in the simulant. The modified AZ-101 interstitial liquid, as shown in Table 4-2, was utilized for these tests and is considered to be a conservative estimate of the AZ-101 interstitial liquid composition.

Table 4-2: **Chemical Composition of AZ-101 Simulant**

Source Chemical	1999 AZ-101 Interstitial Liquid Sample (M)	2018 BBI for AZ-101 Interstitial Liquid Sample (M)	Modified AZ-101 (M)
Sodium hydroxide	0.68	0.42	0.0818
propionic acid	NA	NA	0.00075
Sodium aluminate	0.3	7.07	0.025
Sodium fluoride	0.12	0.32	0.120
Sodium nitrite	1.60	1.04	1.60
Sodium nitrate	0.83	0.58	0.826
Potassium nitrate	0.12	0.07	0.12
Trisodium phosphate, 12-hydrate	0.02	0.08	0.020
Sodium sulfate	0.23	0.38	0.050
Sodium carbonate	0.57	1.1	0.570
Sodium chromate	NM	NM	1.00E-03
Boric acid	NM	NM	1.00E-03
Pitting Factor	4.61	1.95	1.91

NM-Not measured. Component was not measured in sample, but necessary for simulant preparation.

4.2.2 AZ-101 Insoluble Solids (Sludge) Simulant Preparation

The FY22 underdeposit corrosion testing was performed utilizing an AZ-101 sludge simulant. The HLW Precipitated Hydroxide nominal simulant preparation was developed by SRNL in 2003 to reproduce the chemical and physical properties of the AZ-101 sample processed by Battelle Pacific Northwest National Laboratory in 2000 [19, 20]. The simulant was comprised of four major components (Al, Fe, Si, Zr) as hydroxides or as oxides with known particle properties (density and size). Simulant preparation was based on a process designed to mimic the manner the solids precipitated in the waste tank. The principal steps in the recipe are:

1. Hydrated manganese dioxide was generated by reacting permanganate ion and manganese (II) ion. The compounds and amounts on a per liter basis are shown in Table 4-3. Fine black solids were produced in this step.

Table 4-3: Compounds for preparation of hydrated manganese dioxide solids. These are dissolved in 1 liter of water.

Compound	Formula	Mass (g)
Potassium Permanganate	$KMnO_4$	1.913
Manganese Nitrate Solution, 50 wt.%	$Mn(NO_3)_2$	6.60

2. The transition metals, lanthanides and alkaline earth metals were added as nitrates or chlorides to the hydrated manganese dioxide solids. The compounds and the amounts are shown in Table 4-4. All compounds dissolved in the solution except for the manganese dioxide solids. The pH was approximately 1.3.

Table 4-4: Compounds for transition metals, lanthanides, alkaline earth metals.

Compound	Formula	Mass (g)
Ferric Nitrate	$Fe(NO_3)_3 \cdot 9H_2O$	453.86
Nickel Nitrate	$Ni(NO_3)_2 \cdot 6H_2O$	15.348
Zirconyl Nitrate	$ZrO(NO_3)_2 \cdot 6H_2O$	75.012
Cerium Nitrate	$Ce(NO_3)_3 \cdot 6H_2O$	5.034
Lanthanum Nitrate	$La(NO_3)_3 \cdot 6H_2O$	5.612
Neodymium Nitrate	$Nd(NO_3)_3 \cdot 6H_2O$	4.042
Barium Nitrate	$Ba(NO_3)_2$	0.891
Calcium Nitrate	$Ca(NO_3)_2 \cdot 4H_2O$	13.708
Cadmium Nitrate	$Cd(NO_3)_2 \cdot 4H_2O$	12.335
Chromium Nitrate	$Cr(NO_3)_3 \cdot 9H_2O$	5.450
Cobalt Nitrate	$Co(NO_3)_2 \cdot 6H_2O$	0.195
Cupric Nitrate	$Cu(NO_3)_2 \cdot 2.5H_2O$	0.662
Magnesium Nitrate	$Mg(NO_3)_2 \cdot 6H_2O$	5.036
Lead Nitrate	$Pb(NO_3)_2$	0.856
Rhodium Nitrate	$Rh(NO_3)_3$, Solution with 4.933 wt.% RH	3.221
Ruthenium Trichloride	$RuCl_3$ 41.74 wt.% Ru	1.188
Strontium Nitrate	$Sr(NO_3)_2$	2.554
Zinc Nitrate	$Zn(NO_3)_2 \cdot 6H_2O$	0.391
Silver Nitrate	$AgNO_3$	0.004

3. While measuring the pH of the solution, 8 M sodium hydroxide was added to precipitate the metal hydroxides/oxides. The pH was greater than 10.

4. 0.6 M sodium carbonate solution (approximately 400 ml) was added to convert the more soluble hydroxides (e.g., calcium and magnesium) to carbonates. The final pH at this step was approximately 12. The solids were greenish-black as shown in Figure 4-1:.

Figure 4-1: Precipitate solids after the addition of the sodium carbonate.

5. The solids were allowed to settle for approximately 2 weeks. During this process the sludge changed color from blackish-green to reddish orange (See Figure 4-2:), which was indicative of the transition from $Fe(OH)_3$ to Fe_2O_3.
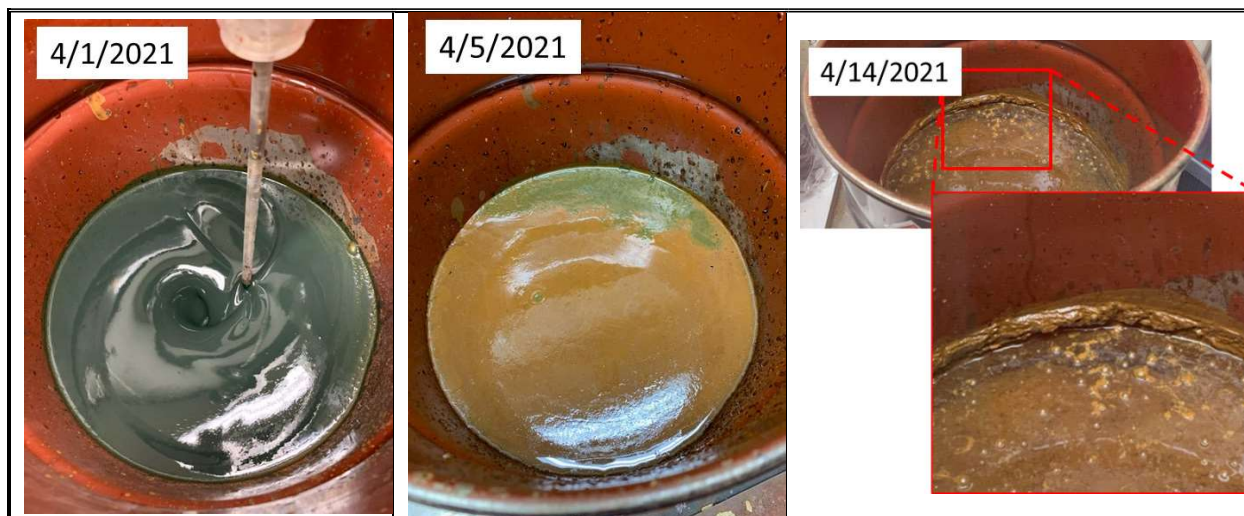
Figure 4-2: Change in precipitate solids during settling.

6. The insoluble solids were washed with inhibited water (0.01 M NaOH and 0.01 M $NaNO_2$) to remove excess soluble sodium, nitrate, and carbonate ions. This process was accomplished by a) the liquid layer above the settled solids was decanted, b) inhibited water was added back and mixed for approximately 30 minutes, c) the solids were allowed to settle and then d) steps a) through c) were repeated until the nitrate concentration was approximately 1000 mg/l. Figure 4-3: shows the pump and mixer set-up for the washing the solids.

Figure 4-3: Set-up for washing with inhibited water.

7. At the completion of washing, the liquid above was decanted until the sludge slurry was approximately 10-11 wt.% solids. At this point there was approximately 16 liters of precipitate slurry.

8. Hydroxide-reactive insoluble species of known particle size were added to the 11 wt.% sludge slurry and mixed thoroughly for 30 minutes. The compounds, amounts, and their particles sizes are shown in Table 5-5.

Table 4-5: Metal oxides/hydroxides used in AZ-101 sludge simulant

Material	Product Name	Mass (g)
Aluminum Oxide, 99.5%	Fine Powder	58.5
Silica, SiO_2	Silicon (IV) Oxide, 99.5%, -400 mesh	8.66
Tin (IV) Oxide	Tin (IV) Oxide, -325 Mesh, 99.9%	1.42
Titanium Dioxide	Titanium (IV) Oxide < 5 μm, 99.9%	0.092

9. The sludge slurry was placed in a heated vessel with a condenser. The slurry was boiled at 102-103 °C for 6 to 7 hours to raise the total insoluble solids concentration to greater than 20%. Figure 4-4: shows the sludge slurry before and after the concentration step. A close-up of the sludge slurry simulant is shown in Figure 4-5:. Approximately 8 liters of sludge was prepared for these tests. The process took approximately 45 days.
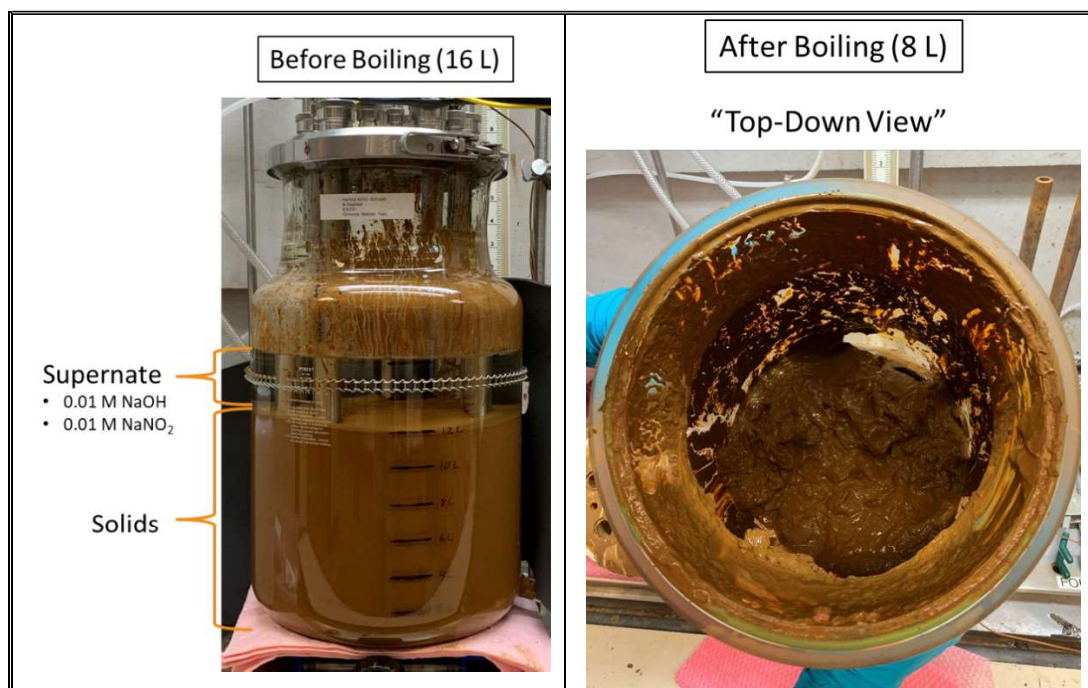
Figure 4-4: Sludge slurry as it is evaporated.

Figure 4-5: Final sludge slurry product.

An SEM micrograph of the undissolved solid particles is shown in Figure 4-6:. The final sludge slurry was also characterized for particle size, wt.% solids, and sludge slurry density. These values were compared to the same values that were measured for the 2000 AZ-101 core sample and the 2003 SRNL simulant that was produced. The particle size distribution for each sludge slurry is shown in Figure 4-7:. The distributions are presented two ways: a) percentage in a channel (i.e., for a given diameter, the percentage of the total number or volume that are at that diameter.) and b) the cumulative distribution of particle size diameter. The 50th percentile diameter for each was compared and is shown Table 4-6. In addition, the wt.% insoluble solids and the sludge slurry density are also shown in the table. The 50th percentile for the 2021 sludge simulant was approximately 8.3 µm, whereas the 50th percentile for the actual 2000 sludge was approximately 3.3 µm. The distributions indicate that there were several large solids particles (~100 µm) present in the 2021 sludge, whereas there were no particles sizes greater than 30 µm measured for the 2000 sludge. It is possible that some particle agglomeration occurred with the 2021 sludge. Particle agglomeration seems even more likely with the 2003 SRNL simulant. In this case the 50th percentile particles size was nearly 25 µm, and large particles near 250 µm were measured.
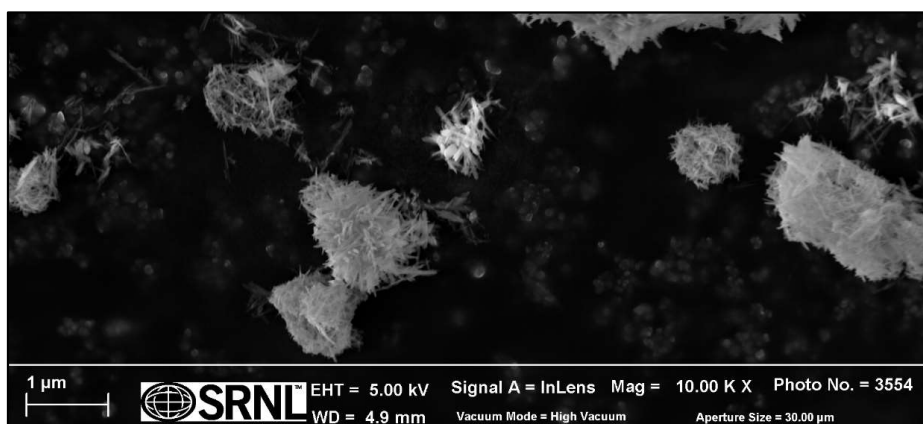
Figure 4-6: SEM micrograph of sludge particles.

(a)

(b)

(c)
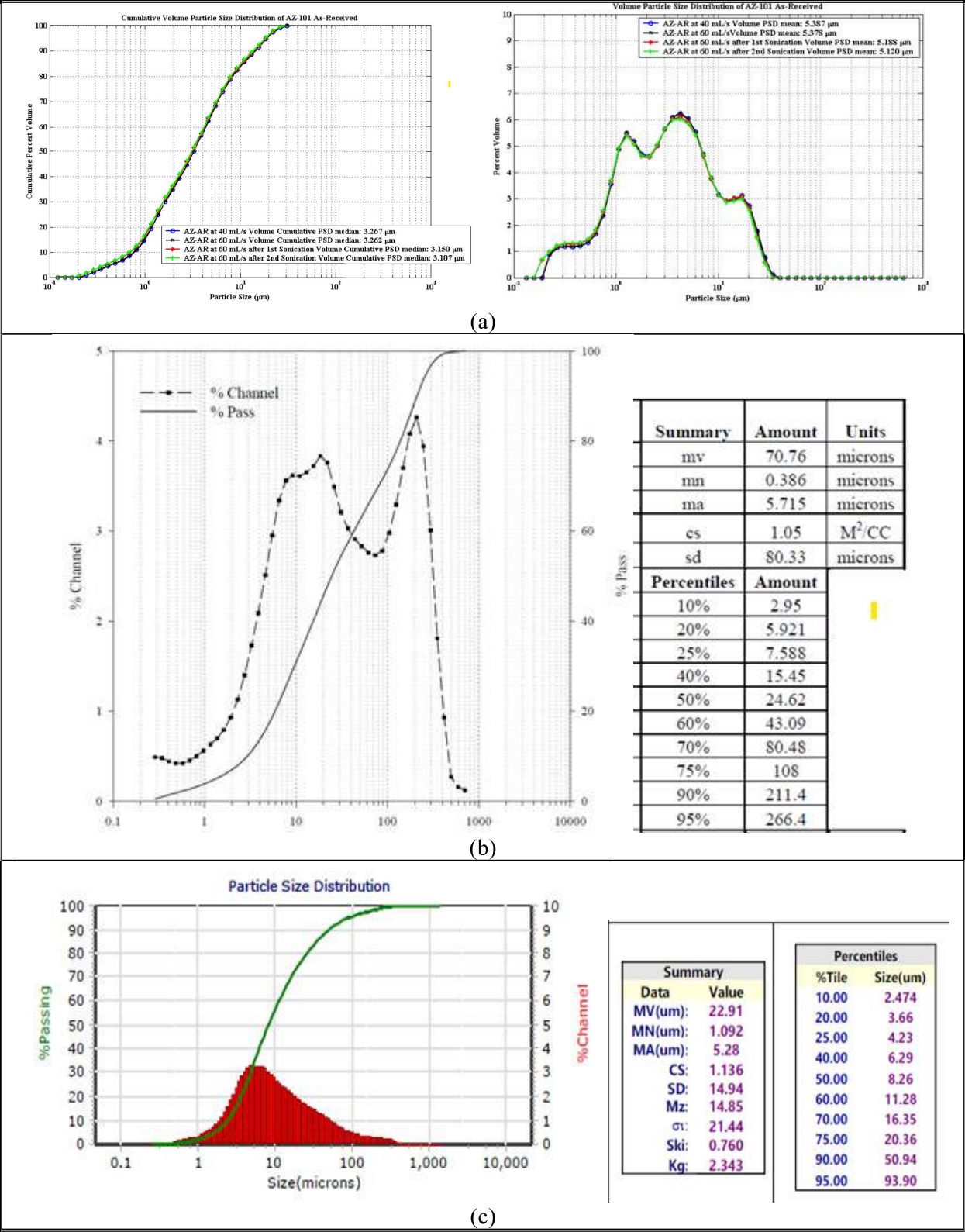
Figure 4-7: Particle size distributions for a) 2000 core sample of AZ-101, b) 2003 AZ-101 sludge simulant, and c) 2021 AZ-101 insoluble solids simulant

The evaporation step concentrated the sludge slurry and was designed to achieve a similar wt.% solids and sludge slurry density that was measured for the 2000 core sample. Table 4-6 shows that these parameters for the sludge simulants compare very well with that of the actual sample.

Table 4-6: Comparison of Sludge Slurry Parameters

Sludge	50% Particle Size (µm)	Sludge Slurry Density (g/ml)	Wt.% Solids
2000 AZ-101 Core Sample	3.3	1.25	25.6
2003 AZ-101 SRNL Sludge Simulant	24.62	1.22	25.8
2021 AZ-101 SRNL Sludge Simulant	8.26	1.23	25.1

4.2.3 Set-up for Short-Term Electrochemical Tests

Several unique setups were used for short-term electrochemical testing. Various combinations of interstitial liquid simulant and/or loose sludge were used to simulate different tank bottom environments. AAR TC128 Rail Car Steel disks measuring 3 inches in diameter and 0.125 inches thick were used for testing. Insulated lead wires were affixed to the back surface of each coupon using conductive silver epoxy to ensure a proper electrical connection to the electrode. The coupons were then mounted in a two-part clear epoxy solution (EpoKwick® from Buehler) so that the electrical connection was protected from the environment and only the top surface of the carbon steel coupon was exposed to the test environment. These mounted samples were then placed in the glass vessels shown in Figure 4-8 with the lead wire exiting the vessel through one of the ports.

In the case of tests conducted with interstitial liquid simulant only, approximately 300 mL of AZ-101 interstitial liquid simulant (described in Section 4.2.1) was added to the test vessel. A salt bridge was inserted into the vessel containing 0.1 M sodium nitrate solution, which provided an ionic pathway for measuring potential of the test coupon using a saturated calomel reference electrode (SCE). Two different types of counter electrodes were used throughout these tests. Initially, two graphite rods served as counter electrodes for the system. Due to issues with available cathodic area, a stainless-steel mesh plunger (described below) was used in subsequent experiments. In the case of the stainless-steel plunger, the salt bridge for the reference electrode protruded through the wire mesh to eliminate any interference of the wire mesh with potential measurements. All ports were then sealed to mitigate loss of water through evaporation. Test vessels were heated to 70 ± 2 °C using a hot plate. The electrodes were connected to the leads of a potentiostat with the lead wire for the carbon steel coupon connected to the lead for the working electrode, the graphite rods (connected with a jumper wire) or stainless-steel plunger connected to the lead for the counter electrode, and the saturated calomel electrode attached to the lead for the reference electrode. Once the test temperature in the vessel was reached, the sequence of electrochemical tests described in Section 4.2.6 was conducted.

In the case of tests involving loose sludge, AZ-101 Insoluble Solids (Sludge) (described in Section 4.2.2) was added prior to the AZ-101 Interstitial Liquid Simulant. Approximately 300 grams of sludge was added for each test, followed by approximately 100 mL of interstitial liquid simulant. The sludge was used in two different configurations. The first was as-received or loose sludge, in which the sludge was not confined and was permitted to freely mix with the interstitial liquid. The second configuration involved compressed sludge, in which the stainless-steel mesh plunger compressed the sludge such that it may not freely mix

with the interstitial liquid and is confined to a defined volume. Images of the plunger and compressed sludge configuration are shown in Figure 4-8. A cross-sectional diagram of the cell configuration is also shown in Figure 4-9.
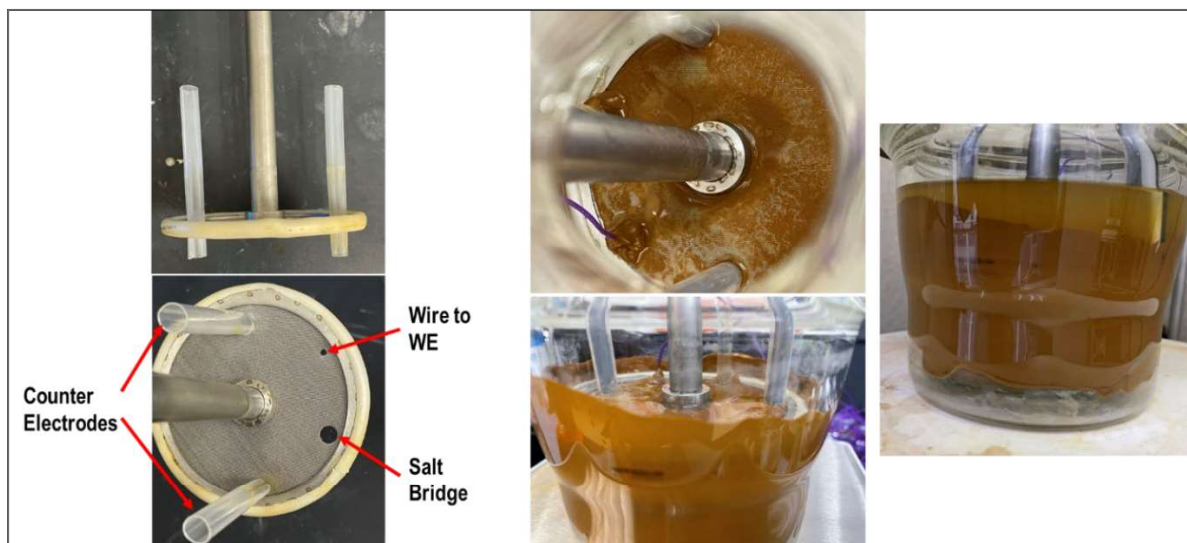
Figure 4-8: Images of Stainless-Steel Mesh Plunger and Compressed Sludge Configuration

Orange – Metal Coupon
Yellow- Adherent Sludge
Green- Wet Sludge
Red – Plunger with Sieve
Purple- AZ-101 liquid
Blue- Crevice Former
White – Insulated Sleeve for CE

Heat
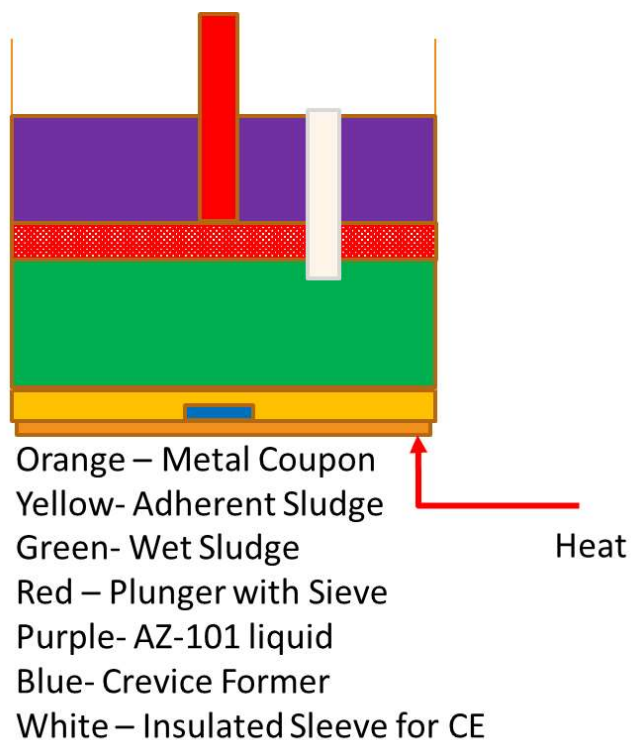
Figure 4-9: Cross-sectional diagram of short-term electrochemical setup.

Similar to the case with testing in interstitial liquid only, two different counter electrode configurations were used. Initially, two graphite rods were used, with the rods protruding through the mesh plunger

insulated by non-conductive plastic sleeves. Due to issues with available cathodic area for the graphite counter electrodes, the plunger itself was used as the counter electrode in subsequent tests. With the exception of the aforementioned differences, the test setup was identical to that of the tests involving interstitial liquid only. Vessels were heated to 70 ± 2 °C, and the sequence of electrochemical tests described in Section 4.2.4 was conducted.

4.2.4 Testing Sequence for Short-Term Electrochemical Tests

The testing sequence for short-term electrochemical tests consisted of a series of four distinct electrochemical techniques: open circuit potential measurements (OCP), linear polarization resistance (LPR), electrochemical impedance spectroscopy (EIS), and cyclic potentiodynamic polarization (CPP) [23-28]. The testing sequence followed the order shown below:

1. 2-hour OCP measurement
2. LPR
3. 30-minute OCP measurement
4. EIS
5. 30-minute OCP measurement
6. CPP

The parameters used for the LPR, EIS, and CPP techniques are shown below:

LPR
Scan Range: ± 20 mV vs. OCP
Scan Rate: 0.167 mV/s

EIS
Frequency Range: 100 kHz – 10 mHz
Perturbation: ± 10 mV
Points per Decade: 7

CPP
Forward Scan
Starting Potential: -100 mV vs. OCP
Final Potential: 1.2 V vs. SCE
Scan Rate: 0.167 mV/s
Current Density Limit: 1 mA/cm^2
Reverse Scan
Scan Rate: -0.167 mV/s
End Potential: 0.0 V vs. OCP

The OCP, LPR, and EIS techniques were performed at or near open circuit and do not disturb the working electrode surface. These techniques preceded the CPP technique which polarized the coupon away from the OCP and can damage the coupon surface irreversibly. In addition, an OCP measurement was placed between each technique to track evolution with time and ensure relative stability of the system. Following the electrochemical tests, the coupon was removed from the test environment and rinsed with distilled water to remove sludge, deposited salts, or any loosely adhered corrosion products. Samples were then visually observed for signs of localized corrosion with select samples being analyzed with a laser confocal microscope (LCM) for surface profiling and characterization of corrosion.

4.2.5 Testing Matrix and Sequence for Long-Term Exposure Tests

Three vessels were fabricated by the SRNL glass shop for the long-term exposure tests. Figure 4-10 presents front and top view images of one of the vessels. The vessels were approximately 10.5" high and approximately 4" in diameter. Ports were formed on the lid in order to insert electrodes for the electrochemical tests, a thermocouple, a condenser, and for solution addition.
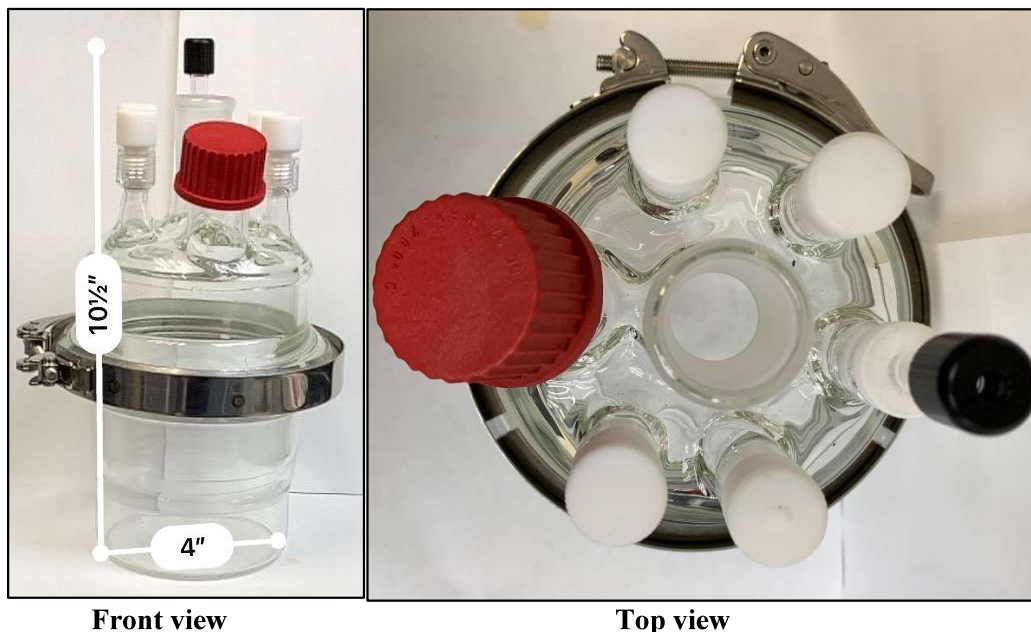
Front view   **Top view**

Figure 4-10: Glass vessel used for underdeposit testing: Front view with dimensions at the left; Top view at the right showing the seven different ports on the lid.

The experiments were conducted using a 3-inch diameter × 0.125-inch thick coupon fabricated from AAR TC 128 steel plate. An insulated wire was attached to the back of the coupon using silver epoxy to provide electrical connection only for the coupons used for the electrochemical tests. The coupons were mounted in a mold prepared with a two-part clear epoxy solution (EpoKwick® from Buehler) so that one face of the coupon was exposed to the test electrolyte. Prior to mounting, each coupon was weighed so that the weight change at the end of the tests could be recorded. A total of three tests were conducted. Details of each test are listed in Table 4-7.. All tests were conducted at 70 °C and atmospheric pressure, with the exposure being for four months.

The following process was used to form an adherent sludge layer and add extra sludge to obtain the desired water content [21]. As-prepared sludge was mixed with the modified supernate solution portions for each experiment in three separate glass vessels. The three mixtures were placed in separate glass vessels and baked in a vacuum oven at 150 °C for one week. The glass vessels were weighed several times during the baking process to ensure that a constant mass was achieved, which correlated with a constant water content. Following completion of the baking, additional as-prepared sludge was added to each vessel to obtain desired moisture content of the composite sludge layer in each experiment. The amount of material used for each experiment of the test matrix is listed in Table 4-8.

Table 4-7: Test Matrix for Long-Term Underdeposit/Crevice Corrosion

Experiment	Deposit Condition	Moisture content
1	Adherent AZ-101 insoluble solids deposit completely covering the coupon with additional AZ-101 sludge.	70
2	Adherent AZ-101 insoluble solids deposit completely covering the coupon with additional AZ-101 sludge.	60
3	Adherent AZ-101 insoluble solids deposit completely covering the coupon with additional AZ-101 sludge, a hole was drilled through the middle of the coupon and a crevice former was installed.	70

Table 4-8: Material Amounts Used to Setup the Long-Term Underdeposit Tests

	Experiment		
	1	2	3[a]
Desired Water Content (percent)	70	60	70
Initial as prepared sludge, used to make the baked sludge layer (g)	67.896	61.147	59.814
AZ-101 Simulant mixed with the as prepared sludge (mL)	600	600	600
Sodium aluminate amount added to the AZ-101 simulant (g)	11.0641	11.0658	11.0666
Mass of the baked sludge (g)	189.43	187.37	188.29
Amount of as prepared sludge added to get the desired water content (g)	375.2	80.1	279.9

[a.] A crevice former was added to the coupon.

The vessels were placed inside the oven on a stainless-steel secondary container. Images were collected during the experiment set up steps; those images are presented in Figure 4-11. A thermocouple was placed inside the furnace and another inside Vessel 2 to record temperatures inside the oven and to have a representative temperature of the sludge inside the vessels. The coupons were exposed to the oven conditions continuously for four months at a temperature of 70 °C. At the completion of the test, the coupons were cleaned and examined for corrosion.

| (a) Image of Vessel 1 after drying the AZ-101 simulant | (b) Image of Vessel 1 after addition of wet, AZ-101 sludge simulant. |

(c) Image of vessels 1 through 3 in the oven.
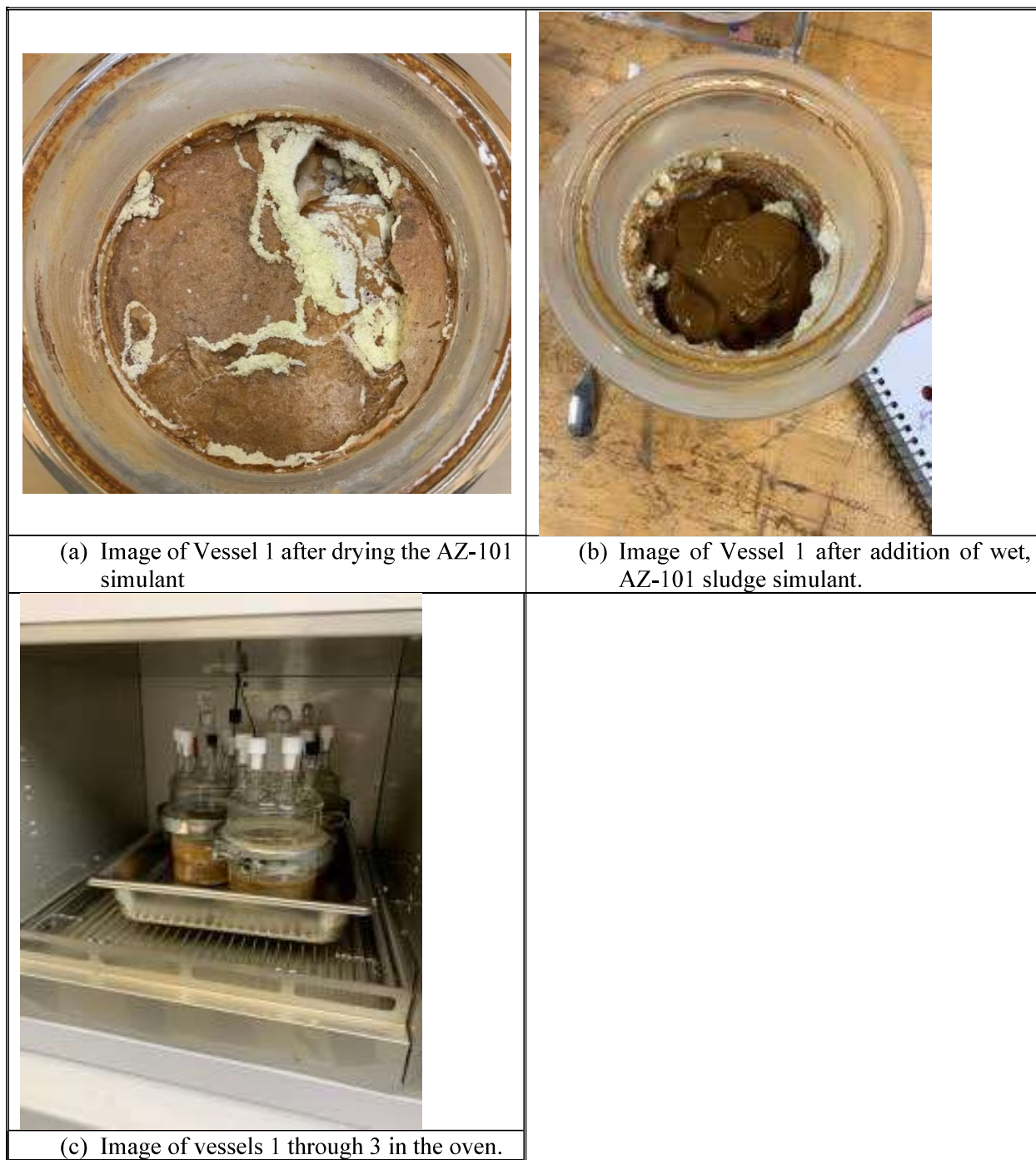
Figure 4-11: Images showing the preparation and set-up of the long-term coupon tests.

4.3 Secondary Liner Corrosion Testing

4.3.1 Materials

Disk coupons, machined from AAR TC 128 steel plate, were used in the secondary liner experiments. The "base" coupons were 25 mm (1 inch) diameter with a thickness of 3 mm (0.125 inch) and polished to a 600-

grit finish. The coupons were mounted in a mold prepared with a two-part clear epoxy solution (EpoKwick® from Buehler) so that one face of the coupon was exposed to the test electrolyte. Prior to mounting, each coupon was weighed so that the weight change at the end of the tests could be recorded. A crevice former was tightly attached to each coupon surface using tape and wire (see configuration in Figure 4-12). The crevice former partially covered the coupon surface, which created conditions for crevice corrosion.
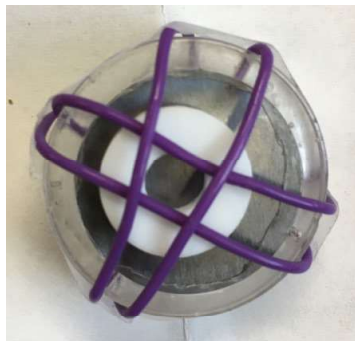
| (a) Top view | (b) Side View |

Figure 4-12: (a) Top, and (b) Side views of the partially covered "base" coupon. The coupon's surface is partially covered with a crevice former, which is held in place using purple wire and tape

4.3.2 Simulant

Groundwater (GW) simulant was used for the secondary liner corrosion studies. The composition of the GW simulant is provided in Table 4-9 and is presented in more detail in Appendix A [22]. The pH of the simulant was adjusted using sodium carbonate and acetic acid to a pH of 7.6. For this test, nitrogen was bubbled though the solution at a rate of 10 sccm.

Table 4-9: Composition of GW Simulant

Chemical	Concentration (M)
Sodium bicarbonate	1.750E-03
Calcium hydroxide	1.500E-03
Potassium nitrate	2.400E-04
Strontium Nitrate	2.874E-06
Ferric sulfate	6.250E-04
Sodium Metasilicate, 5-hydrate	6.000E-04
Ferric chloride	7.667E-05
Manganese Chloride	3.100E-04
Acetic Acid	3.000E-04
pH adjusted using sodium carbonate and acetic acid	7.6

4.3.3 Testing Apparatus

A Glass column that is 3.3 ft tall and 5.5-inch diameter was used for the experiment (see Figure 4-13). Approximately 1 to 1.5 L of simulant was added to a vessel, located at the bottom of the column. The vessel was equipped with a water jacket in which circulated warm water flowed to maintain the temperature at 45 ± 2 °C. The column also has several ports, which were used to insert thermocouples, ER probes, and oxygen concentration sensors. Coupons were suspended from a rod with stainless steel rings at four different levels and exposed to the GW simulant and column vapor space. These levels are described as follows.

Immersed: Coupons are suspended in the vessel simulant for the whole duration of the test (i.e., 6 months). This represents continuous contact between the secondary liner and the groundwater.

Level 1: Bottom or low level. Coupons were dipped in the simulant for five minutes prior to testing. The coupons were hung at the bottom fixed ring of the rod shown in Figure 4-13 (b). These coupons were suspended approximately 1 inch above the liquid level of the simulant. Every two weeks, the coupons were lowered into the simulant for 5 minutes. This level is representative of the secondary liner bottom plate experiencing periodic wetting/drying.

Level 2: Intermediate or middle level. Coupons were dipped in the simulant for five minutes prior to testing. The coupons were hung at the middle-fixed ring approximately 18 inches above the liquid simulant in each vessel. This level is representative of a vapor space region of the secondary liner bottom that at one time was exposed to water, but since then has had infrequent or no contact with water. However, this region is exposed to the humidified air that may re-dissolve soluble salts that exist on the metal surface.

Level 3: Top or high level. This set of coupons was not exposed to the solution prior to testing. The coupons were suspended approximately 36 inches above the simulant. This level is representative of the secondary liner bottom plate region that is only exposed to the humidified air and any volatile species from the solution.

Initially, the coupons at each level were exposed to the GW simulant only for 78 days, without any nitrogen. The GW simulant was then purged with nitrogen starting on the 78th day of the experiment; the purging continued for the next 120 days. In addition, simultaneous to the start of nitrogen purging, another set of polished coupons at each level were loaded in the experimental vessel; three coupons each at Levels 1, 2, and 3, and four coupons immersed in GW. This step investigated the influence of the nitrogen purge alone on carbon steel corrosion. Leaving a few of the coupons that had been exposed for 78 days investigated the effect of nitrogen on mitigating corrosion that had already initiated. Furthermore, when nitrogen was added to the vessel, a port on the top lid of the vessel was fitted with a tube that passed through a water trap; this allowed flow of the nitrogen through the vessel. The dissolved oxygen concentrations were measured in the GW simulant and water trap. In addition, the oxygen concentration was also measured in the outflow gas that passed through the water trap.

(a)   (b)

Figure 4-13: Images of the (a) experimental configuration, and (b) steel rod to suspend the coupons

4.4 Quality Assurance

Data for all Tasks were recorded in the electronic laboratory notebook system, notebook number J1719-00476-03, J1719-00476-04 and G1720-00424-06.

Requirements for performing reviews of technical reports and the extent of review are established in manual E7 2.60. SRNL documents the extent and type of review using the SRNL Technical Report Design Checklist contained in WSRC-IM-2002-00011, Rev. 2.

5.0 Results and Discussion

The results and discussion for the report are enumerated by the corresponding task.

5.1 Underdeposit Corrosion Testing

5.1.1 Long-Term Exposure Tests

The corrosion rates as determined by weight loss are listed in Table 5-1. No significant difference in the corrosion rates is apparent. The rates are also low and typical of well inhibited solutions [11].

Post-test images of the coupons are presented in Figure 5-1. After cleaning the sample, the polishing marks on the sample were easily visible, which again demonstrates that limited attack occurred. However, a closer examination of the surface revealed the presence of tiny defects that were uniformly distributed on the surface of the coupons.

To investigate the severity of these defects the coupon surfaces were profiled using a laser confocal microscope (LCM). Each coupon was profiled using a 10x magnification lens in 10 parts. For each part, the profiled coupon surface was corrected for curvature. Given the complex curvature on the coupon surface, it was not possible to correct each part using a given curvature correction method; therefore, each part was realigned by selecting the correction methods that provided the most useful information about the defects or micropits. The profiled images of Coupon 1 parts are presented in Figure 5-2. To understand the extent of micropitting on the Coupon 1 surface, a line profile was obtained for each part of Coupon 1; the line profile data for the ten parts of Coupon 1 are provided in Table 5-2. The surface roughness range before exposure was approximately ± 1.5 μm; as seen in Table 5-2, several micropits developed on Coupon 1 surface during the long-term exposure. The profiled images of Coupon 2 are presented in Figure 5-3, and the line profile data for the various parts are provided in Table 5-3. Similarly, the profiled images of Coupon 3 parts are presented in Figure 5-4, and line profile data for those Coupon 3 parts are provided in Table 5-4.

The profiled images indicate that the density of these micropits was slightly greater for Coupons 1 and 3 compared to Coupon 2. No accelerated attack was observed in the area beneath the crevice former that was attached to Coupon 3. For comparison, the deepest pit depths for each part on Coupons 1-3 are listed in Table 5-5.

Table 5-1: Long-Term Test Coupon Corrosion Rate Data

Coupon	Deposit Condition	Moisture Content (percent)	Corrosion rate (mpy)
1	Adherent AZ-101 insoluble solids deposit completely covering the coupon with additional AZ-101 sludge.	70	1.12
2	Adherent AZ-101 insoluble solids deposit completely covering the coupon with additional AZ-101 sludge.	60	0.82
3	Adherent AZ-101 insoluble solids deposit completely covering the coupon with additional AZ-101 sludge, a hole was drilled through the middle of the coupon and a crevice former was installed.	70	1.92

Coupon 1	Coupon 2	Coupon 3
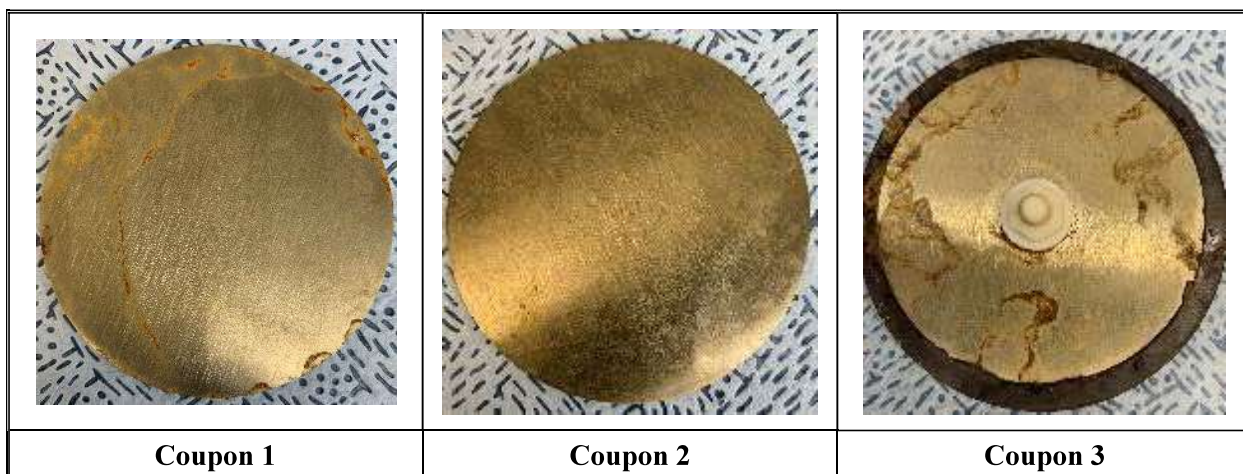
Figure 5-1: Post-test images of the long-term underdeposit coupons
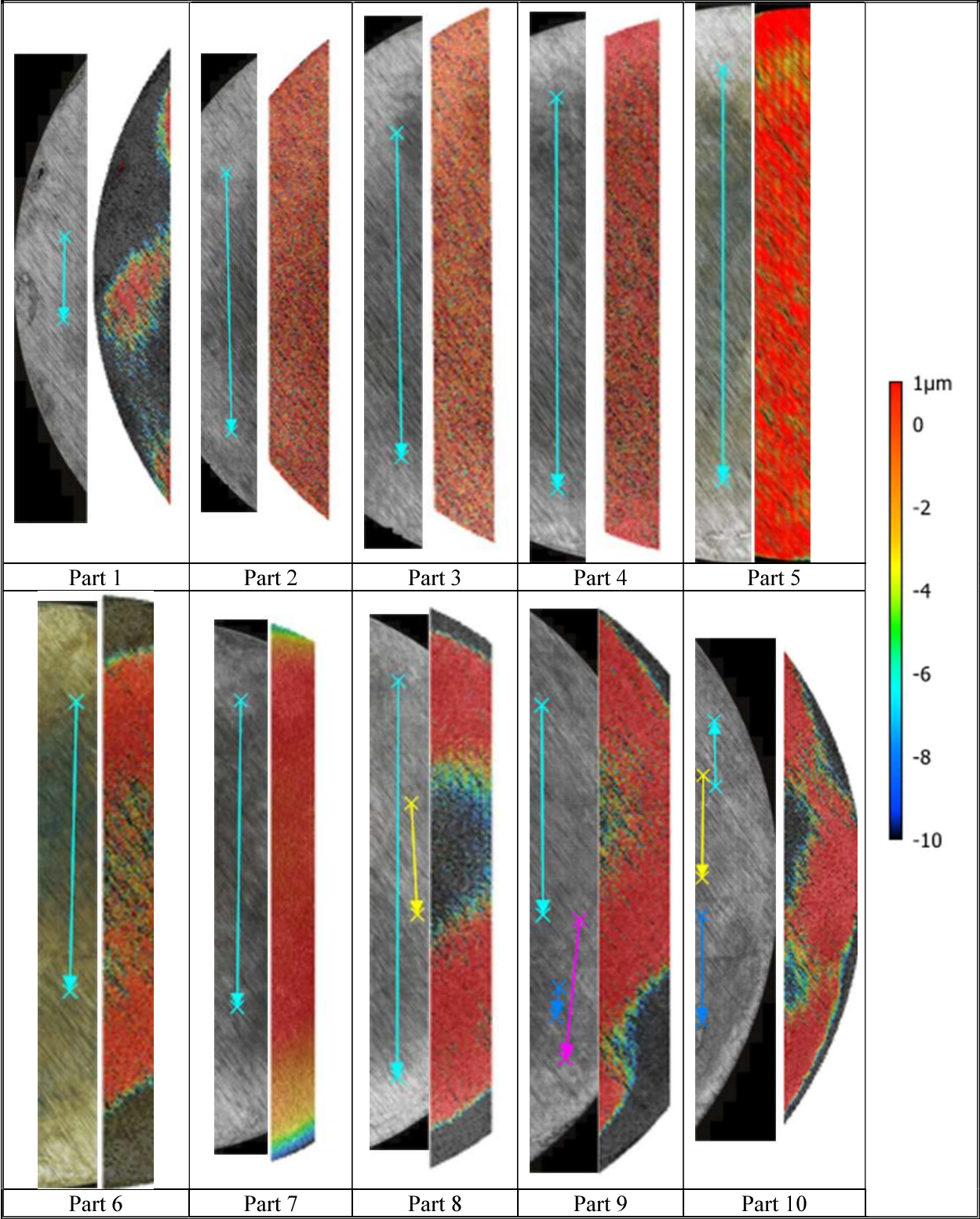
Figure 5-2: Camera and profiled images of Coupon 1 parts.

Table 5-2: Line Profile Depth Data for Various Parts of Coupon 1
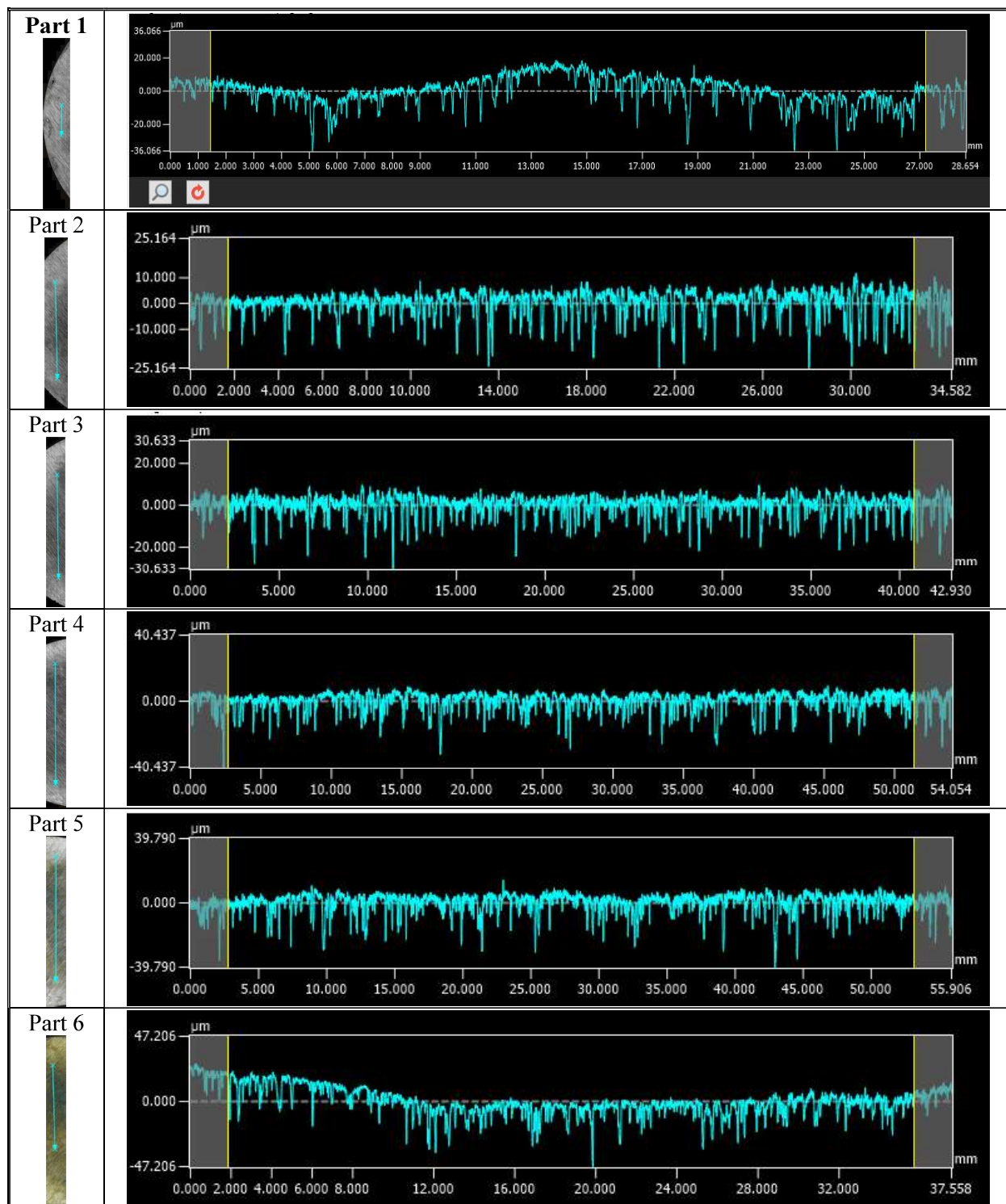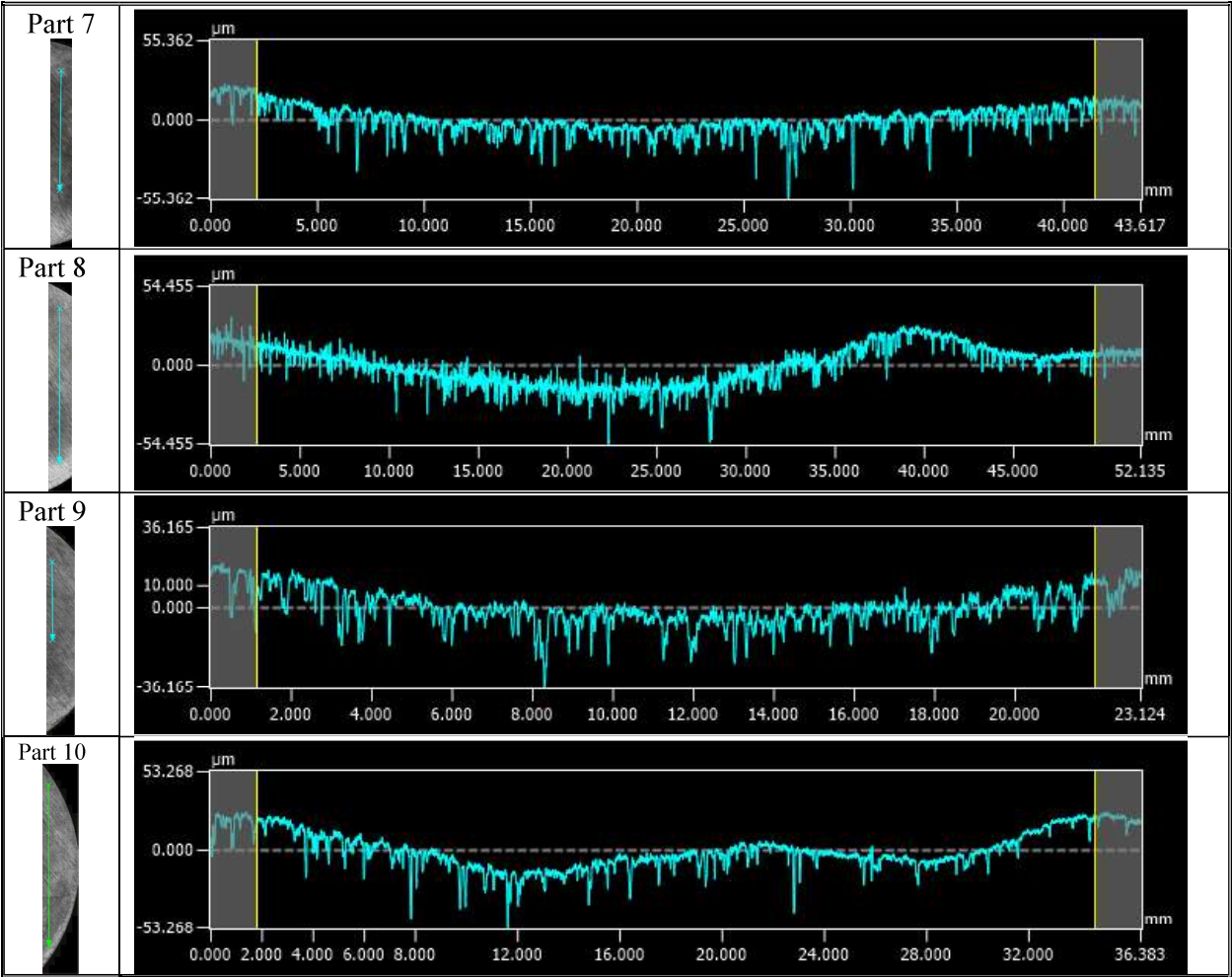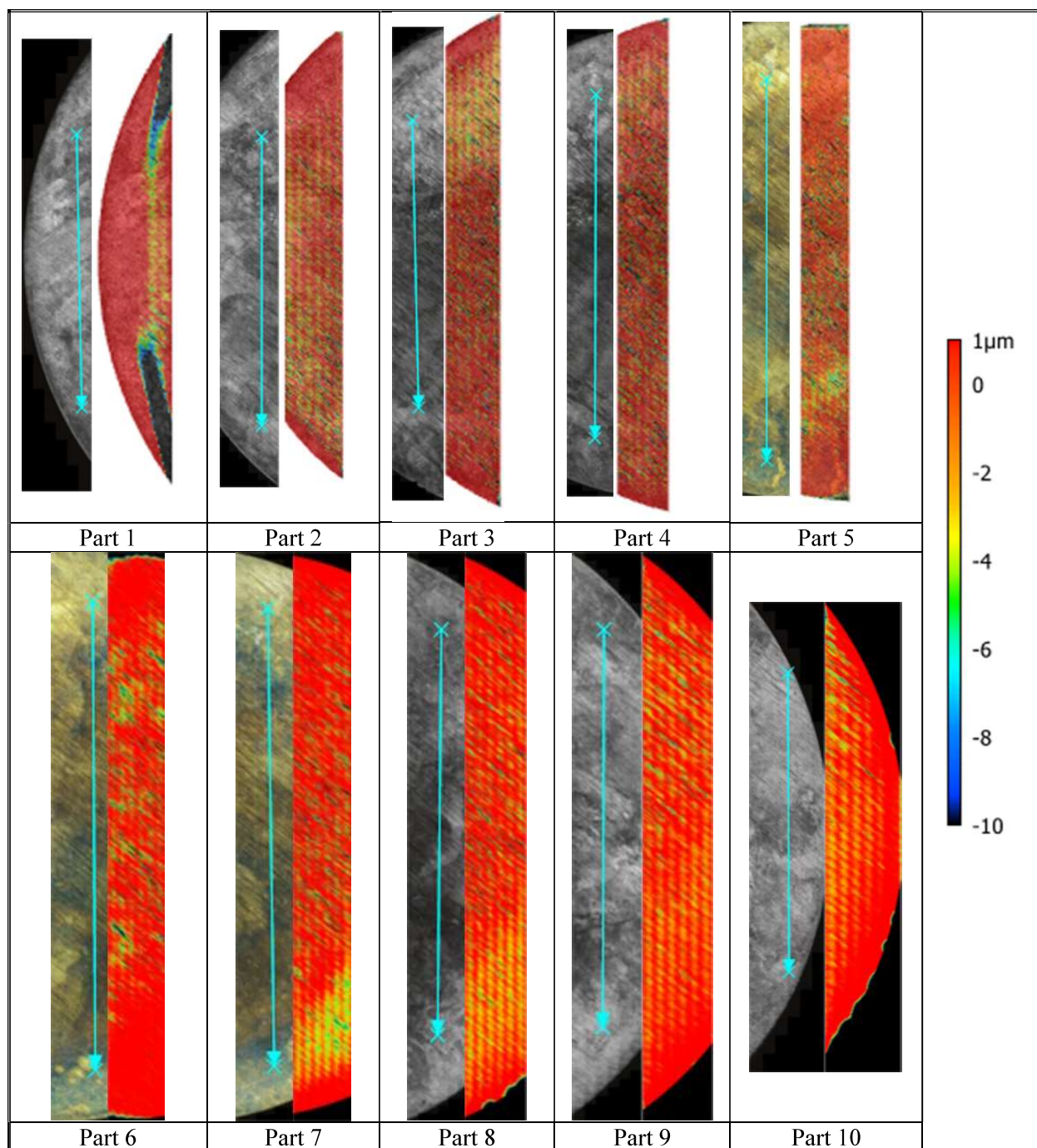
Figure 5-3: Camera and profiled images of Coupon 2 parts.

Table 5-3: Line Profile Depth Data for Various Parts of Coupon 2

Part 7	
Part 8	
Part 9	
Part 10	
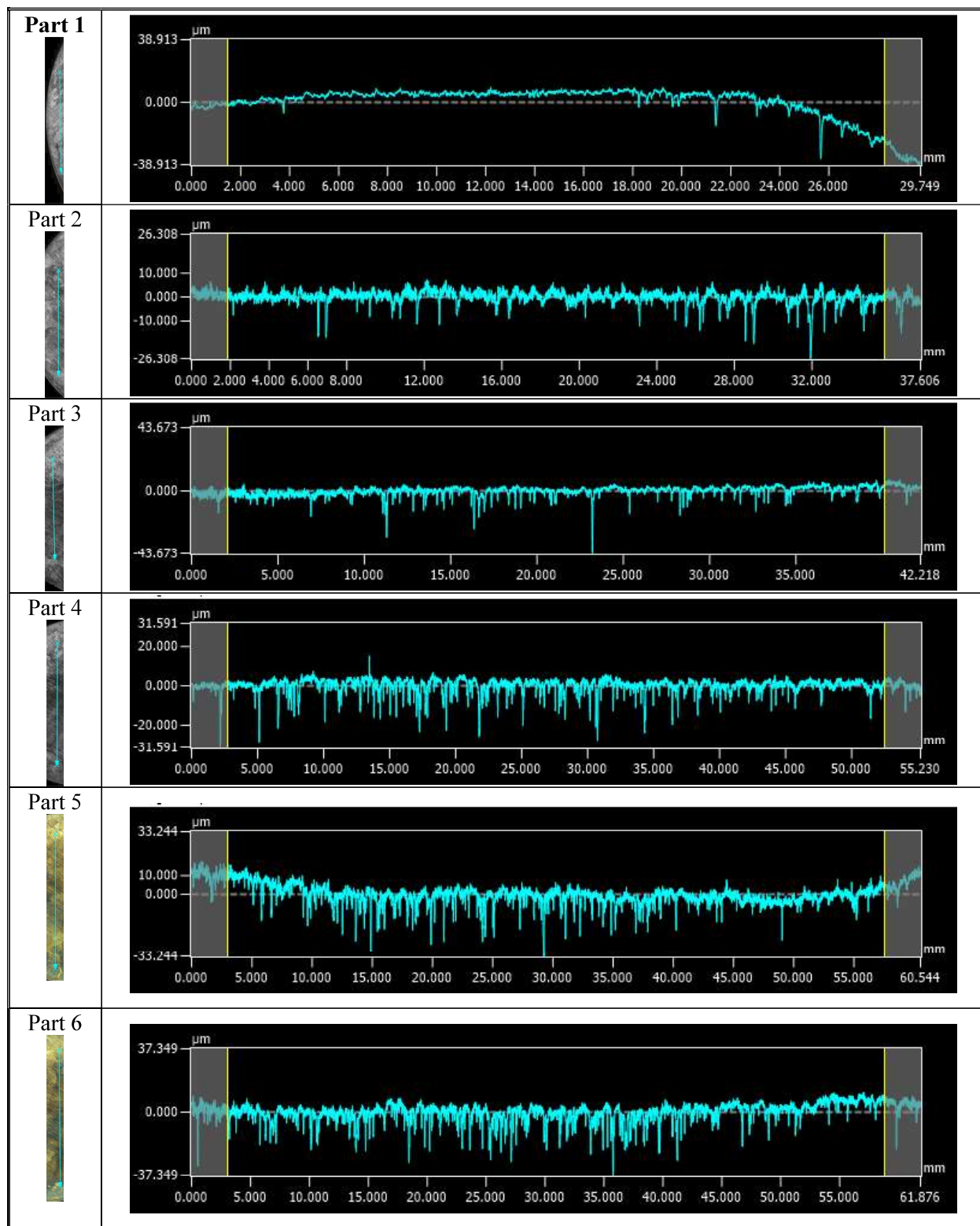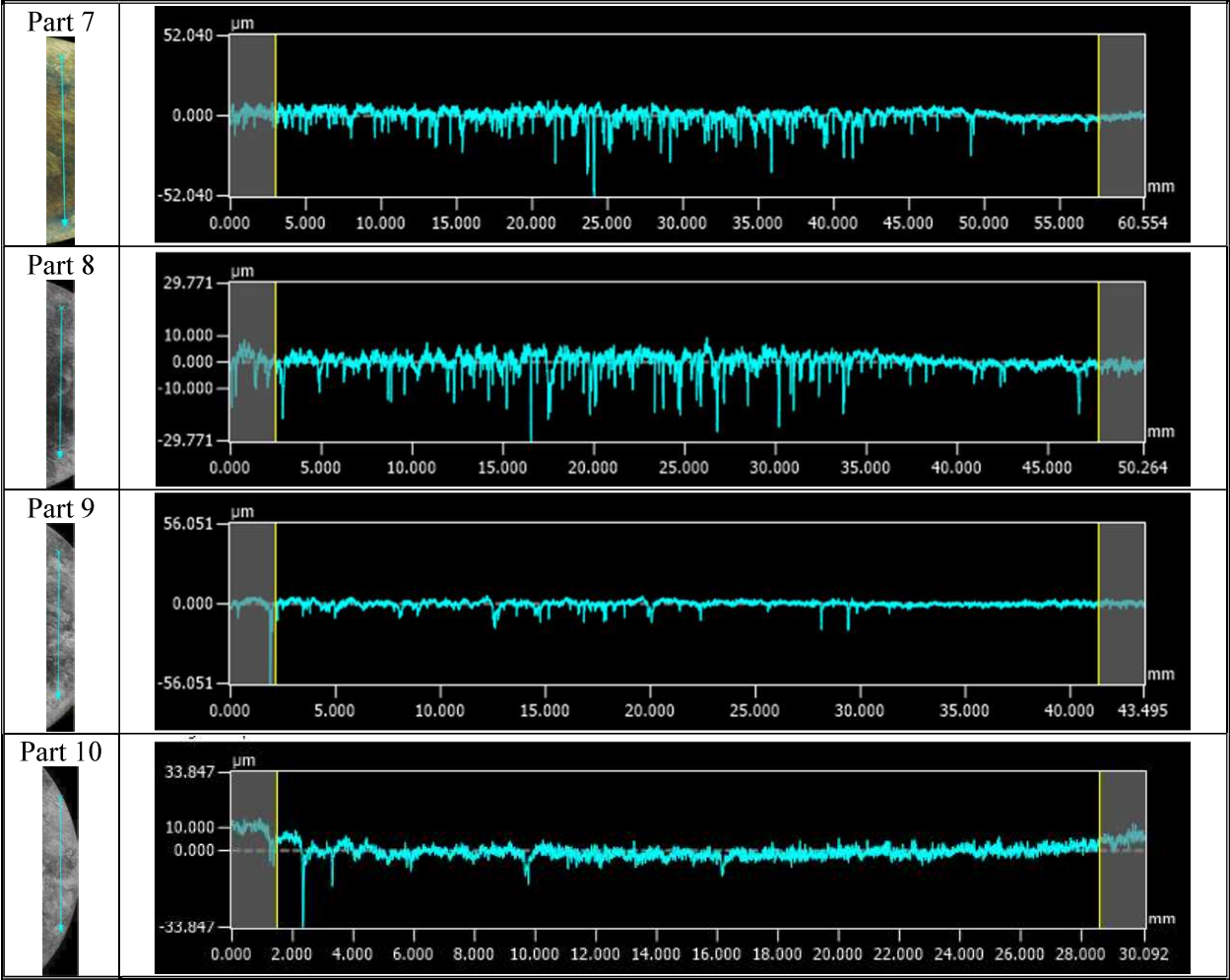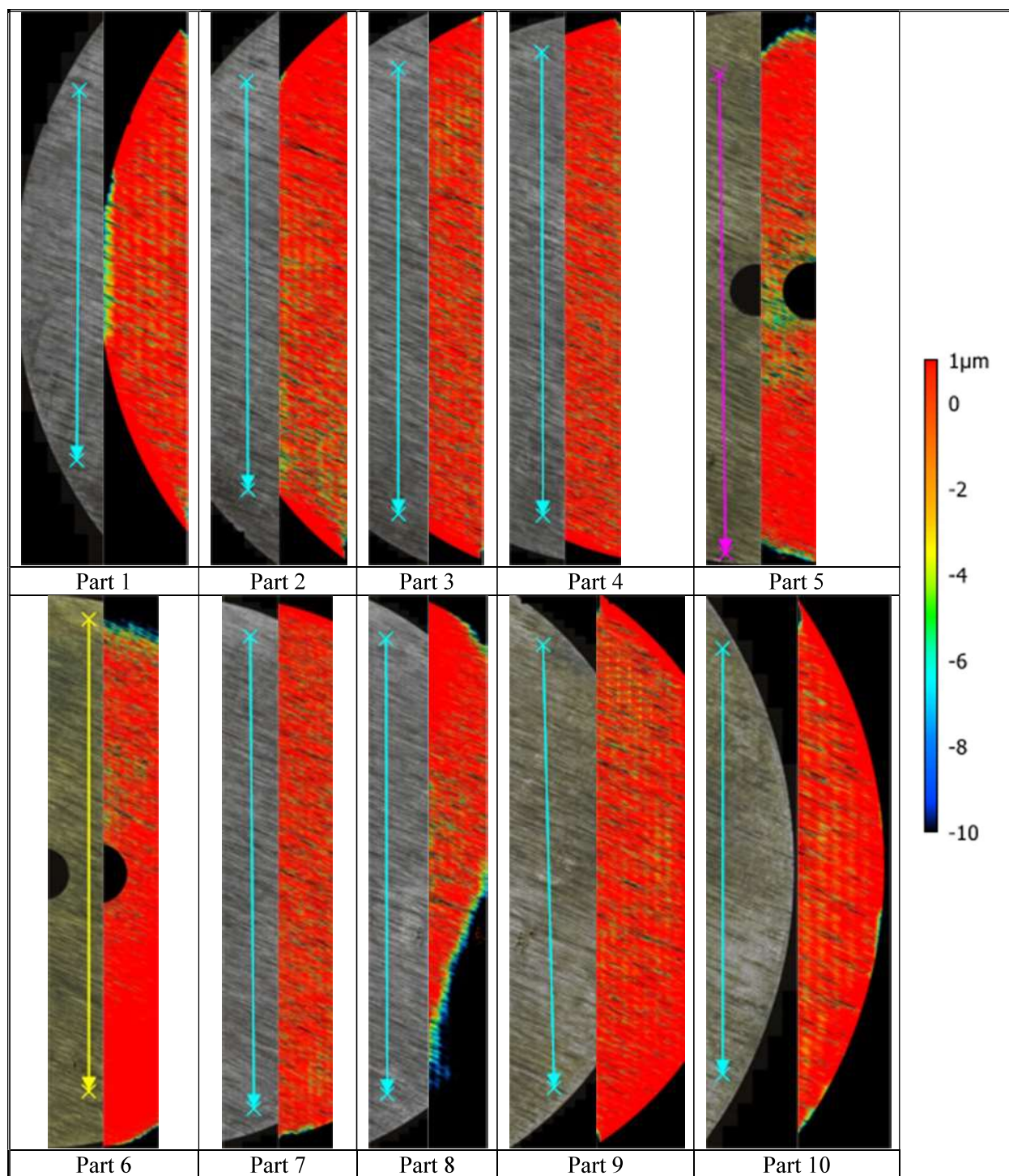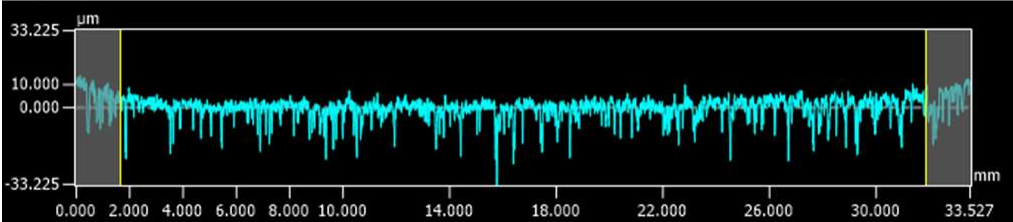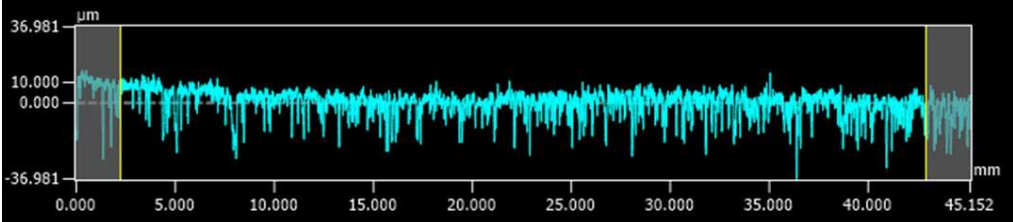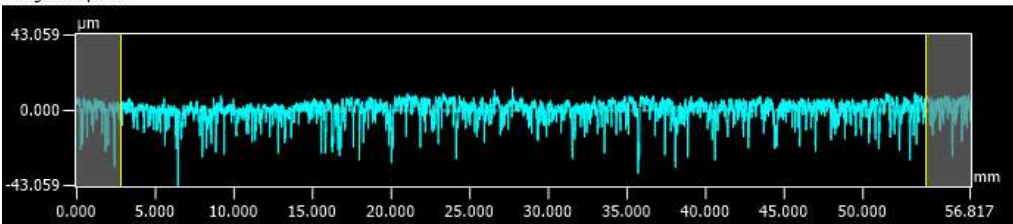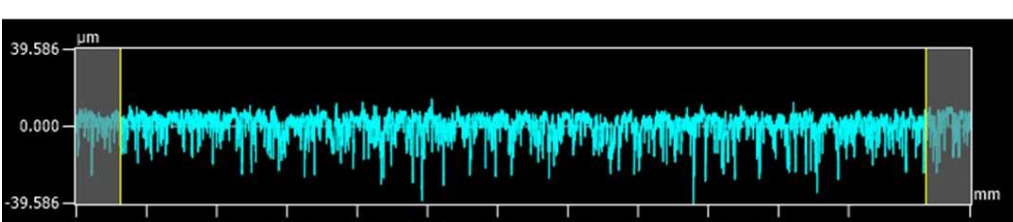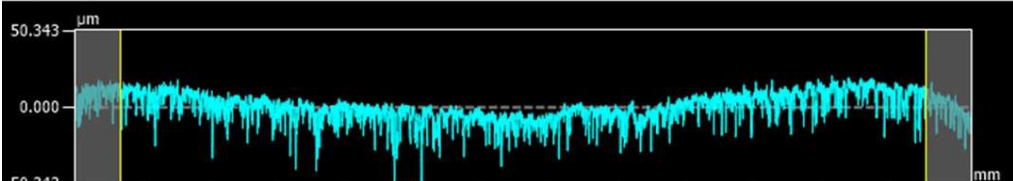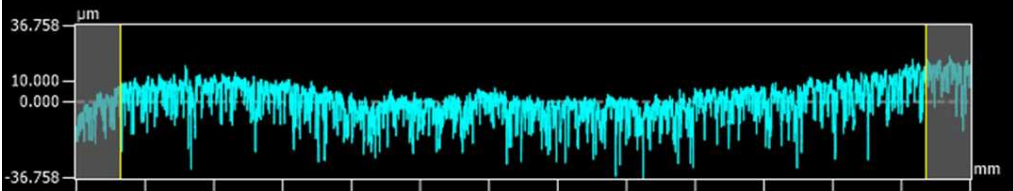
Figure 5-4: Camera and profiled images of Coupon 3 parts.

Table 5-4: Line Profile Depth Data for Various Parts of Coupon 3

Part 1	
Part 2	
Part 3	
Part 4	
Part 5	
Part 6	

Part 77
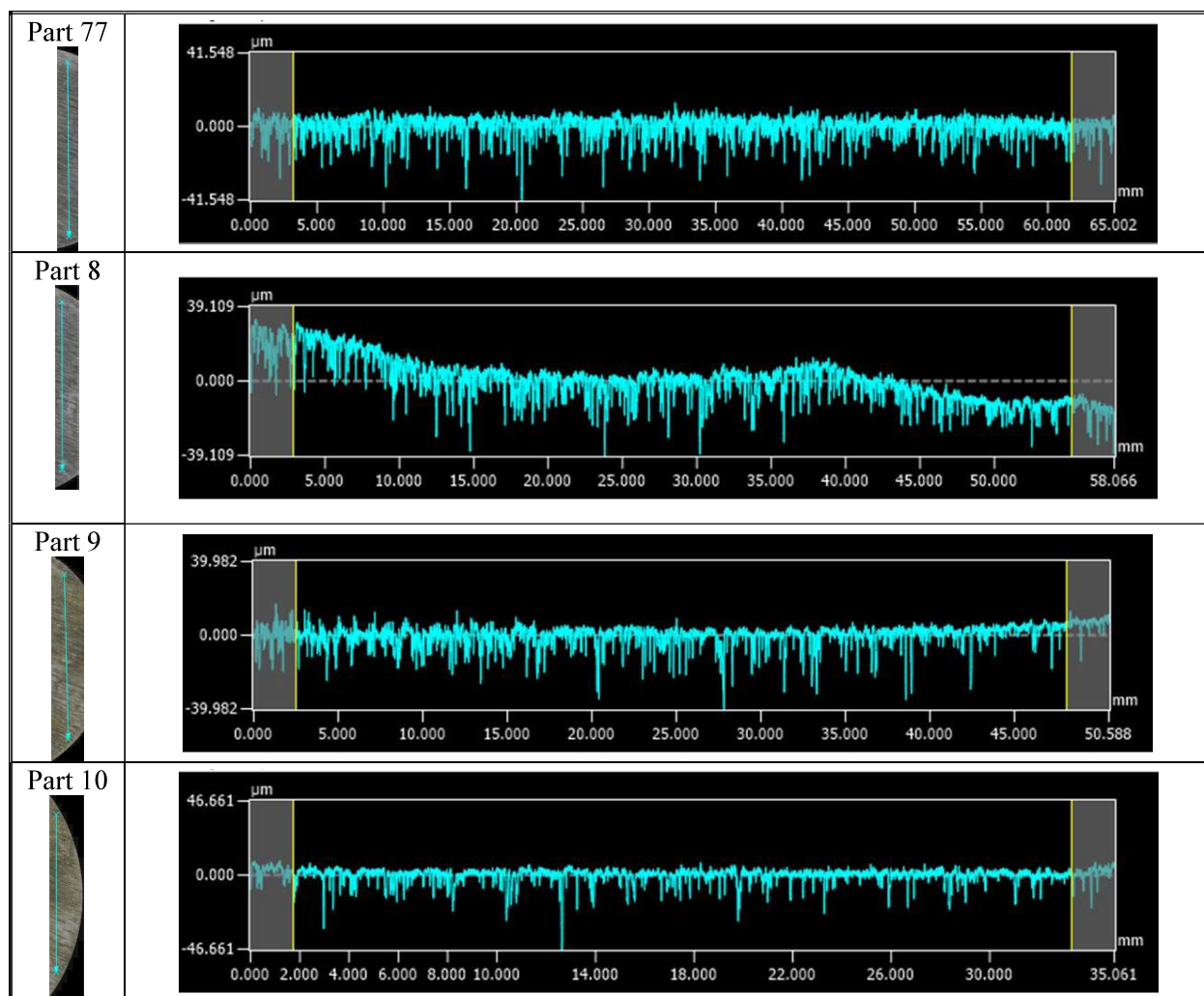
Part 8

Part 9

Part 10

Table 5-5. Deepest Pit Depths (μm) for Various Parts of Coupons 1, 2, and 3. Numerical values in parentheses are in mils.

| Coupon	Part 1	Part 2	Part 3	Part 4	Part 5	Part 6	Part 7	Part 8	Part 9	Part 10
1	125 (4.92)	54 (2.13)	50 (1.97)	64 (2.52)	62 (2.44)	142 (5.59)	227 (8.94)	112 (4.41)	128 (5.04)	69 (2.72)
2	178 (7.01)	55 (2.17)	49 (1.93)	60 (2.36)	57 (2.24)	57 (2.24)	66 (2.60)	58 (2.28)	62 (2.44)	54 (2.13)
3	50 (1.97)	50 (1.97)	61 (2.40)	51 (2.01)	101 (3.98)	73 (2.87)	62 (2.44)	168 (6.61)	51 (2.01)	58 (2.28)

Cumulative distribution plots for the deepest pits on each coupon were prepared to assess the severity of the attack and compare the maximum pit depths for each coupon. To create the plot, the deepest pit depths on each coupon were ranked from smallest to largest (i.e., from 1 to 10). The cumulative fraction was then calculated for each maximum pit depth. The cumulative fraction is calculated by dividing the rank by the total number of pits, in this case 10. These manipulations are illustrated in Table 5-6, while the cumulative distribution plots are shown in Figure 5-5. Three fractions from this plot were utilized to compare the

distributions: 0.5, 0.9, and 1.0. These fractions are highlighted in yellow in Table 5-6 as well. The distribution of maximum pit depths for Coupons 2 and 3 are very similar. The distribution of pits on coupon 1 was similar up to the 0.5 fraction, but slightly deeper at the 0.9 and 1.0 fraction. However, the difference between these values is relatively minor. Therefore, the effect of the water concentration at the levels tested on both general and localized corrosion is not significant.

Table 5-6. Cumulative Distributions for Maximum Pit Depths (mils) for Coupons 1, 2, and 3.

Rank	Coupon 1	Coupon 2	Coupon 3	Cumulative Fraction
1	1.97	1.93	1.97	0.1
2	2.13	2.13	1.97	0.2
3	2.44	2.17	2.01	0.3
4	2.52	2.24	2.01	0.4
5	2.72	2.24	2.28	0.5
6	4.41	2.28	2.40	0.6
7	4.92	2.36	2.44	0.7
8	5.04	2.44	2.87	0.8
9	5.59	2.60	3.98	0.9
10	8.94	7.01	6.61	1.0
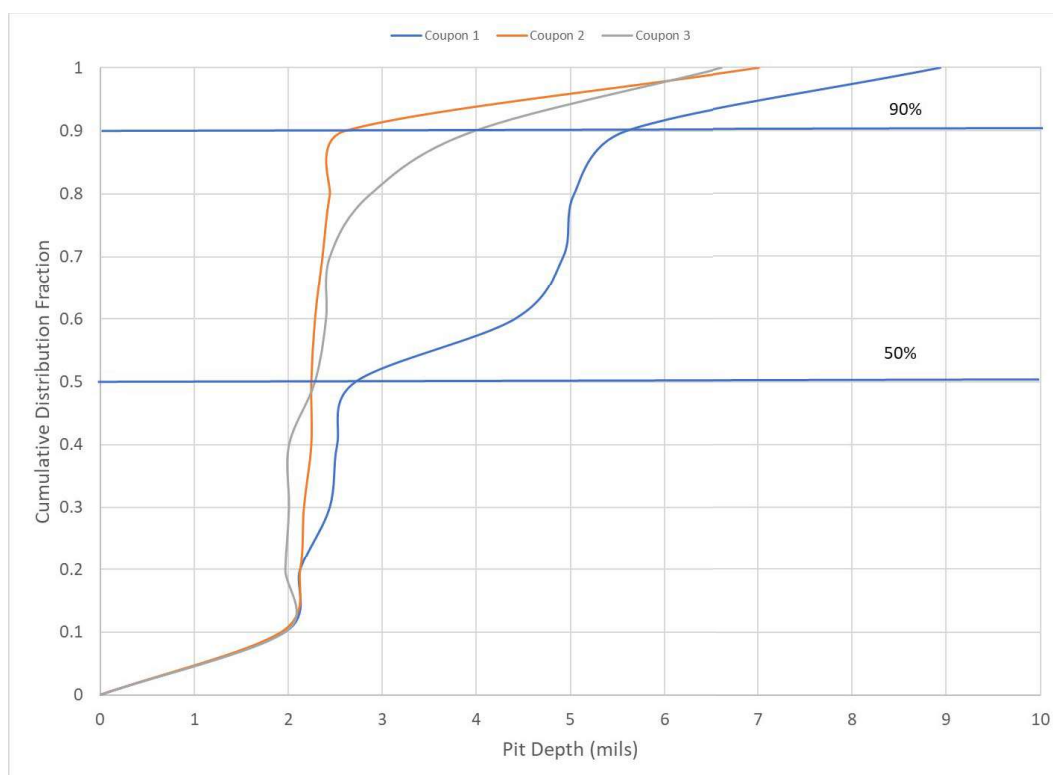
Figure 5-5. Cumulative Distributions for Maximum Pit Depths (mils) for Coupons 1, 2, and 3.

A second consideration is whether these pit depths represent significant attack. Three previous series of tests where pit depths were characterized were evaluated to investigate this question [11, 29]. All tests were conducted for approximately four months. In 1996, Zapp performed immersion tests on carbon steel coupons in an uninhibited solution (pH 9.73, PF = 0.08 at 50 °C). Similarly, in 2018 Fuentes et.al., conducted immersion tests in uninhibited solutions at 35 °C. These latter tests were divided into two categories. The first series of tests, referred to as Fuentes 1 2018, were conducted in low pH solutions (pH 10) over a range of low to moderate PF values (0.0 to 2.11). The second set of tests, referred to as Fuentes 2 2018, were conducted at higher pH (> 13) and low PF (0.81 to 1.04). The pit depths in these latter tests were all termed minor attack. For the exposure tests in 2022, the hydroxide concentration was 0.068 M and the PF was 1.96 at a temperature of 70 °C and solids were present. While there are significant differences in the conditions, the comparison was utilized to illustrate how these recent maximum pit depths compare to what has historically been considered pit depths of concern.

Cumulative distribution fractions for the maximum pit depths in each study were prepared. Figure 5-6 compares the cumulative distribution fractions for these three series of tests and the current 2022 study. The pits from the 2022 study are considerably smaller than those from the Zapp study or Fuentes 1 2018. For the most part, pits from the recent tests are smaller than the pits observed for Fuentes 2 2018, although, the maximum pit depths at the upper end of the cumulative distribution are similar. Thus, these micropit features at most represent minor attack similar to a slightly uninhibited solution.

These observations indicate that these micropits differ from stable, propagating pits. One possibility is that these micropit features initiated early on during the test beneath a solid particle, but stable pit growth was not sustained for the entirety of the test. A possible explanation for this observation is that inhibited interstitial liquid from the wet sludge penetrated through the solids and resulted in repassivation of these small pits beneath the solids.
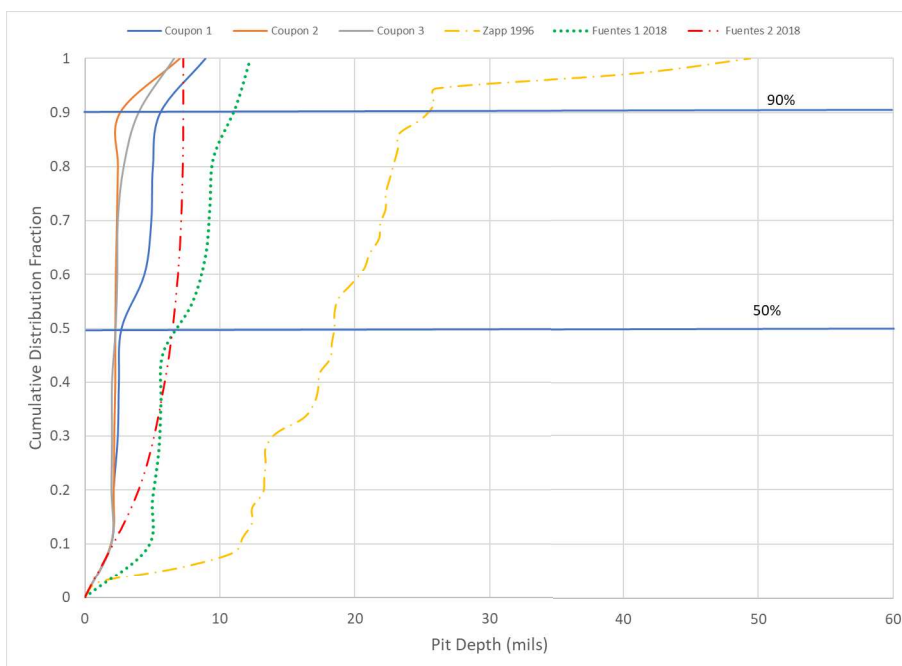

Figure 5-6. Cumulative Distributions for Maximum Pit Depths (mils) for Coupons 1, 2, and 3 and Three Historical Tests.

5.1.2 Short-Term Electrochemical Tests

Three distinct conditions were evaluated in FY22. The first condition was carbon steel coupons exposed to AZ-101 Interstitial Liquid Simulant only. This served as the control condition used to assess the behavior of the material in the absence of any deposited solids. The second was loose sludge that was not compressed, which accounts for the localized chemistry beneath the solids without compaction of the solids that would occur due to the weight of solids and liquid in a storage tank. This condition also allowed for free mixing of the sludge with the liquid simulant. The final condition incorporated compaction and confinement of the insoluble solids that simulates hydrostatic pressure on the solids layer and prevents free mixing of the sludge and liquid layers and creates a condition where the solids are more likely to form adherent solids on the metal surface.

Using the test sequence described in Section 4.2.4, four types of data were generated. The first was the evolution of the OCP with exposure time. The second was LPR, which yields a polarization resistance that is inversely proportional to the corrosion rate. The third type of data is EIS, which yields information about the resistance of the liquid and/or insoluble solids, the capacitance of the system, and the polarization resistance. The final type of data were polarization curves generated from CPP scans. Information about the corrosion potential, passive current density, and presence of localized corrosion may be gleaned from this data.

The sequence of electrochemical tests was applied to four test conditions, which are described in Table 5-7 (see section 4.2.3 for further description of the condition). The test condition will be utilized in the legend of subsequent figures for identification.

Table 5-7 Test Conditions for Electrochemical Tests

Test Condition	Description
AZ-101 Simulant	Testing was conducted in the AZ-101 interstitial liquid simulant as shown in Table 4-2. The tests were performed with graphite counter electrodes. The wire mesh sieve was not present.
AZ-101 Simulant_Sieve CE	Testing was conducted in the AZ-101 interstitial liquid simulant as shown in Table 4-2. The tests were performed with the wire mesh or sieve as the counter electrode. The graphite counter electrodes were not present.
Wet Sludge	Testing was conducted with wet, loose sludge simulant above the coupon. Approximately 100 ml of AZ-101 interstitial liquid was added above the wet sludge. The wire mesh or sieve was utilized as a counter electrode, however, pressure was applied to the sieve in order to confine the solids to a restricted volume and not allow it to mix freely with the AZ-101 interstitial liquid.
Wet Sludge_Not Compressed	Testing was conducted with wet, sludge simulant above the coupon. Approximately 100 ml of AZ-101 interstitial liquid was added above the wet sludge. The sieve was utilized as a counter electrode, however, no pressure was applied to the sieve and thus the wet sludge was allowed to freely mix with the AZ-101 interstitial liquid. Note that at 70 °C, there is sufficient convection that results in suspension of the wet solids in the interstitial liquid as observed in previous tests [15]
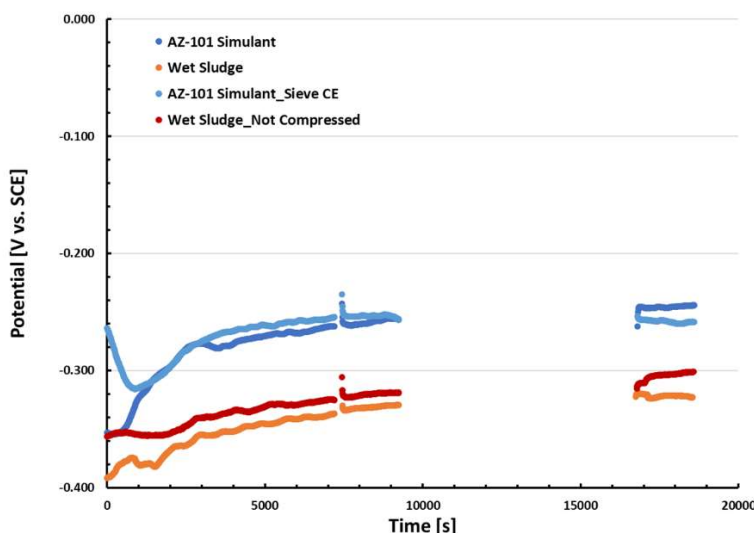
Figure 5-7: OCP evolution with time during short-term electrochemical tests.

Figure 5-7 shows the OCP evolution with time for each test condition. The OCP data illustrates the sequence and time at which the electrochemical measurements were performed. The first 7200 seconds (i.e., 2 hours) illustrates monitoring the OCP of the carbon steel. At 7200 seconds, each test shows a small perturbation in the potential. This represents the 10-minute time necessary to perform the LPR scan. The LPR scan was followed by a 30-minute OCP measurement that allows the coupon to equilibrate with the solution. The gap in the OCP measurement between approximately 9500 seconds and approximately 17,000 seconds represents the time at which the EIS scan was performed. Following the EIS scan, the sample was again allowed to equilibrate with the solution for 30-minutes. During that time, the OCP was measured until the CPP scans were initiated.

The influence of the presence of the mesh on the potential measurements was investigated by comparison of the OCP measured for AZ-101 simulant and AZ-101 simulant_Sieve CE. As can be seen in Figure 5-7, with the exception of the OCP at the onset of the experiment, the values measured at the two test conditions did not differ by more than 20 mV during the sequence of tests. This indicated that use of the mesh plunger as the counter electrode does not interfere with measurement of the potential of the carbon steel coupon in a meaningful way.

The influence of wet sludge on potential measurements was also evaluated by comparing the OCP values for the interstitial liquid and the wet sludge. The presence of the wet sludge resulted in an active shift in the negative direction of approximately $40 - 70$ mV in the potential of the carbon steel coupon as compared to the interstitial liquid . It was also noted that compression of the sludge resulted in a $10 - 20$ mV negative shift in the OCP compared to that of the uncompressed sludge. The shift to more active potentials may be indicative of the initiation of localized or general corrosion beneath the solids.
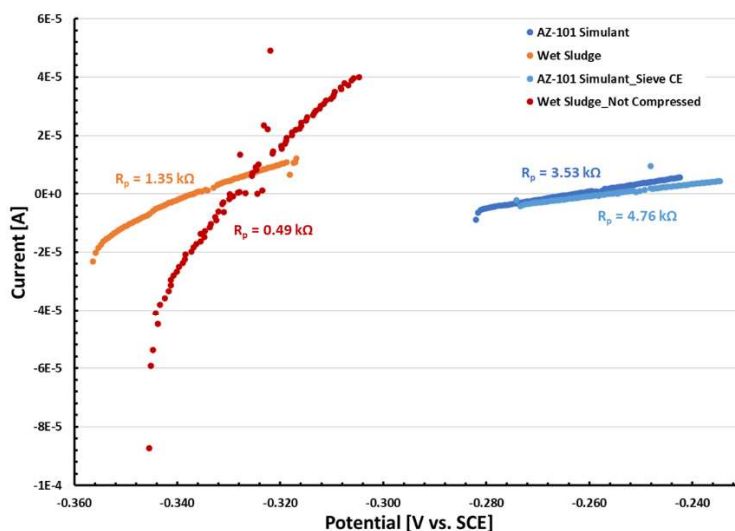
Figure 5-8: LPR data for short-term electrochemical tests

The LPR data generated (presented in Figure 5-8) provides an indication of the relative corrosion rates of the various test conditions at open circuit after the 2-hour exposure. These data reinforced the difference in the OCP between the conditions involving sludge and interstitial liquid only, as a significant offset exists between the potential at zero-current for the two groups.

The slope of the current-potential plot, shown as R_p in Figure 5-8, may be used to calculate the corrosion rate. The corrosion current, I in Amps, is calculated from Equation 1 below [23]:

$$I_{corr} = \frac{B}{\frac{dE}{dI}} \qquad (1)$$

where, B is a constant related to the anodic and cathodic Tafel slopes. A B value of 26 mV is representative for iron in many of these passive caustic environments [24]. The corrosion rate, CR in mils/yr, is calculated from Equation 2 [24]:

$$CR = 0.13\ I_{corr}\ (EW)/d\ (A) \qquad (2)$$

where, EW is the equivalent weight (27.5 g for iron), d is the density (7.86 g/cm^3) and A is the surface area of the sample (45.6 cm^2). The corrosion rates are summarized in Table 5-8. The corrosion rates in all the tests are very low and reflect a well inhibited environment in all cases. The calculated corrosion rates for the two interstitial liquid tests are very similar and indicate once again that use of the wire mesh for the counter electrode did not significantly influence the results of the electrochemical test. The calculated corrosion rates for beneath the wet sludge are slightly higher, but because they are so low and of a similar magnitude it is difficult to distinguish if significant corrosion is occurring beneath the solids.

Table 5-8 Estimated Corrosion Rates for Each Test Condition

Test Condition	R_p (kΩ)	Corrosion Rate (mils/yr)
AZ-101 Simulant	3530	0.073466
AZ-101 Simulant_Sieve CE	4760	0.054482
Wet Sludge	1350	0.1921
Wet Sludge_Not Compressed	490	0.529256
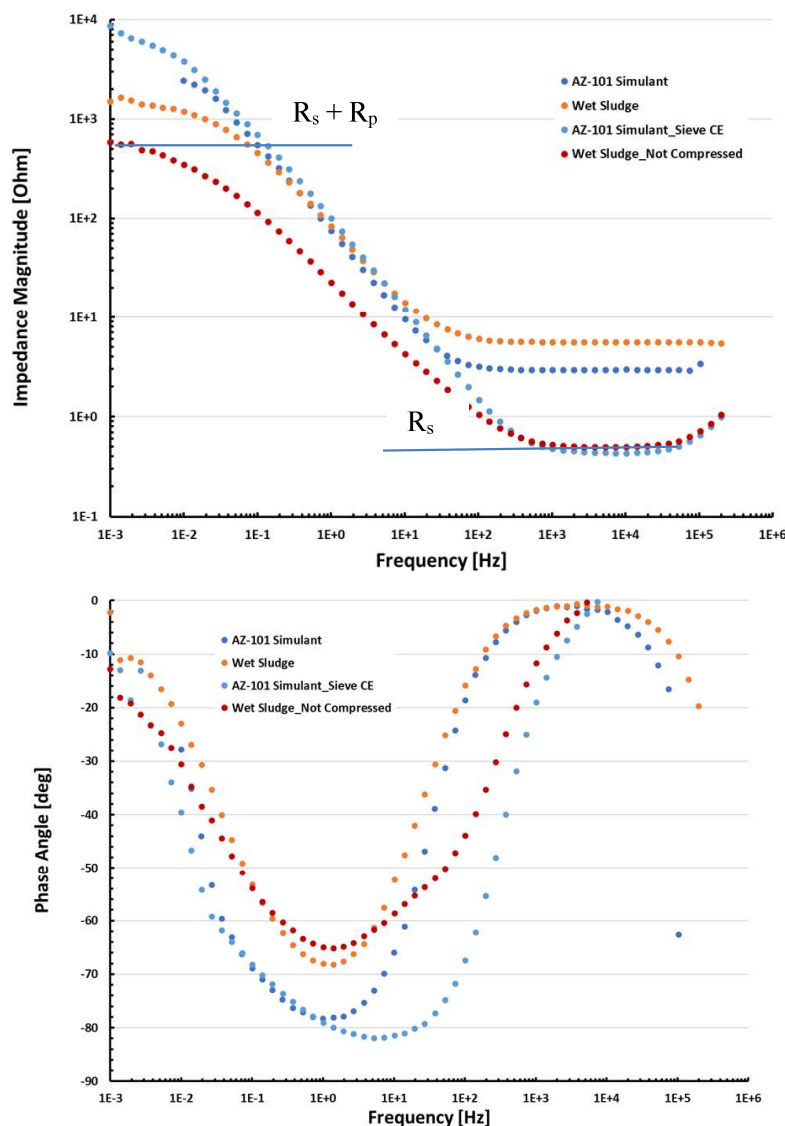
Figure 5-9: Bode plots showing the impedance magnitude (top) and phase angle (bottom) for the short-term electrochemical tests.

Through the EIS data generated, the R_p values obtained from LPR could be corroborated and observations about the conductivity through the sludge layer could be ascertained. These data are presented in the Bode plot in Figure 5-9. Two key parameters were estimated. The solution resistance (R_s) is estimated

from the horizontal portion of the impedance plot at high frequency. Knowing this value, the polarization resistance may be estimated from the horizontal portion of the plot at low frequencies. In this case, R_s is three orders of magnitude less than $R_s + R_p$ at each condition and therefore the impedance at the high frequency is essentially R_p. On the low frequency portion of the scans, it can be seen that the R_p values are between 0.5 to 8 kΩ. It is important to note that these measurements occurred a few hours apart in the exposure, so while the values for each condition are not an exact match, the values being the same order of magnitude and in the same order from highest to lowest indicated good agreement between the two data sets.

Qualitatively, there is only one minimum present in the phase angle plot and only the two plateaus for the impedance plot in Figure 5-9, which corresponds to a single time constant for the electrochemical system [25]. The presence of only one time constant at each condition indicated that the presence of sludge was not influencing the electrical response of the system (electrically distinct layers, localized corrosion processes). The relatively small differences in the low frequency portion of the scans showed that while the sludge was slightly more resistive than interstitial liquid only, the conductivity through the wet sludge was adequate for conducting electrochemical measurements with higher currents without creating a prohibitive potential resistance.

Polarization curves from CPP scans were used to evaluate the localized corrosion behavior of the varying conditions. Figure 5-10 shows the comparison of the two conditions tested in interstitial liquid only: using graphite counter electrodes and using the wire mesh counter electrode. The scan using the graphite electrodes (top) shows the issue encountered when using these as a counter electrode. Despite polarizing the electrode to 1 V, the current density limit of 1 mA/cm^2 could not be obtained. This was attributed to the relatively small cathodic area the electrodes afforded compared to the large area of the 3-inch diameter coupon. The wire mesh of the plunger offered substantially more surface area, and the current limit was able to be obtained at a reasonable potential value. The current during the forward scan of the CPP curve for this test displays some instability indicating that the characteristics of the oxide film are being disturbed. The current on the reverse scan is initially less than that of the forward scan. However, the current on the return scan crosses over the forward scan current at approximately +100 mV and exceeds the forward scan current for the remainder of the test. According to the protocol utilized by SRNL, WRPS, and the CSGto evaluate CPP curves, the result would be classified as a Category 3 or mixed response. This result may indicate the initiation of pits on the forward scan, but later cessation of growth due to repassivation. On the other hand, this may reflect the influence of other ionic species present that are being oxidized or reduced and ultimately influencing the total current that is measured. This possibility cannot be ruled out either given the characteristics of the CPP curve. Another test such as the modified G192, which may elicit more pit growth than the CPP test, may have made a distinction between these two possibilities [30].
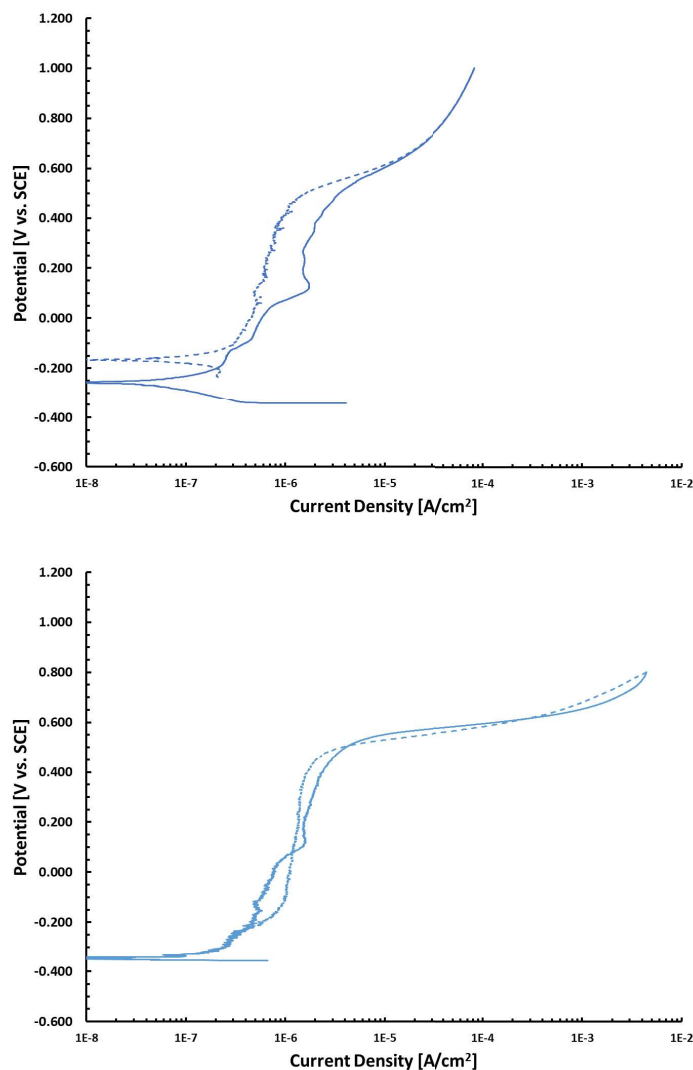
Figure 5-10: CPP curves for AZ-101 Interstitial Liquid Simulant with graphite counter electrodes (top) and plunger counter electrode (bottom). Solid line indicates forward scan and dashed line indicates reverse scan.

Figure 5-11 shows the comparison of the CPP curves for the interstitial liquid only and that of the condition of compressed wet sludge. The CPP curve for the compressed sludge condition exhibited pronounced instability in the forward scan and had positive hysteresis at the initial stage of the return scan (i.e., category 2), indicating pitting, crevice corrosion, or some other type of localized corrosion mechanism. The polarization curve for the compressed sludge condition also indicated repassivation of this localized attack at 290 mV vs. SCE. With this repassivation potential being more than 600 mV higher than the corrosion potential, it is unlikely that this accelerated attack would occur at open circuit given the time interval evaluated. It was also apparent from these tests that the compressed sludge yielded a lower corrosion potential, higher corrosion rate, and a higher passive current density than the interstitial liquid.
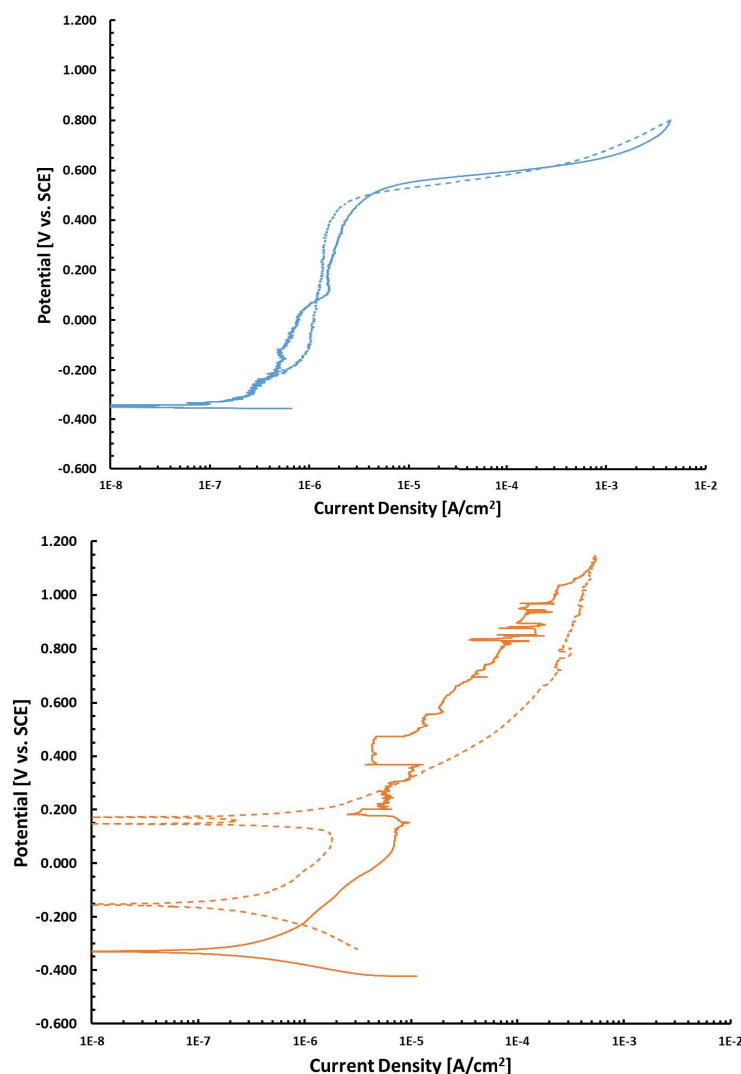
Figure 5-11: Comparison of polarization curves for exposure to AZ-101 Interstitial Liquid only (top) and compressed AZ-101 Sludge (bottom). Solid line indicates forward scan and dashed line indicates reverse scan.

The differences between exposure to loose sludge and to compressed sludge, were also evaluated using CPP. These polarization curves are displayed in Figure 5-12. As stated previously, the compressed sludge condition produced a category 2 CPP response, indicative of the possible initiation of pits, but ultimate repassivation at approximately 290 mV vs. SCE. On the other hand, the loose sludge condition produced a category 1 CPP response (i.e., negative hysteresis), which indicates that no localized corrosion initiated. It is of interest to note that the passive current density on the forward scan did increase with potential indicating some instability in the passive film characteristics, such as the initiation of breakdown. However, it is clear from the reverse scan that the surface has passive characteristics.

Because of the possible indications of localized corrosion observed during the CPP scan, the coupon used for the compressed sludge condition was analyzed for the nature and extent of localized corrosion that occurred. Images of the coupon surface are shown in Figure 5-13.

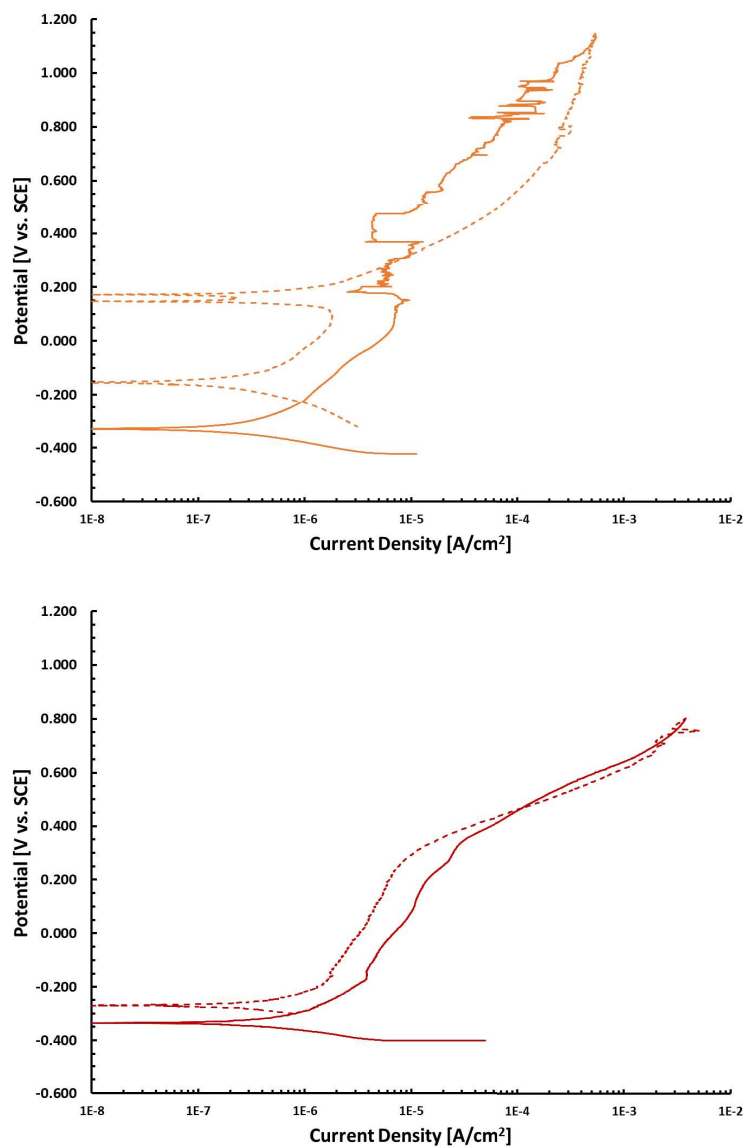**Figure 5-12:** Comparison of polarization curves for exposure to compressed (top) and loose (bottom) AZ-101 Sludge. Solid line indicates forward scan and dashed line indicates reverse scan.

Figure 5-13: Images of coupon following exposure to compressed sludge during the short-term electrochemical test sequence.

When the coupon was removed from the test vessel, loosely adhered deposits were noted on the sample surface. These deposits corresponded to the areas of corrosion attack that can be observed in Figure 5-13. While the majority of the sludge could be removed by simply rinsing the coupon with water, the areas of adhered deposits required physically wiping the surface to remove the sludge. Beneath the deposits were areas that resembled a more general attack in addition to distinct areas of more localized, deeper attack that resembled crevice corrosion (areas that appear darker in the images in Figure 5-13). No pitting was apparent on the surface through visual examination of the sample. Other areas of the sample that were not covered by loosely adhered solids appeared pristine, with the grind marks from sample preparation clearly visible. In order to more clearly analyze the nature of localized attack and to quantify the depth of attack, this sample was analyzed using a LCM.

Figure 5-14 shows the optical image (top left), profile map (top right), and a depth profile across a region of the sample that experienced localized attack beneath loosely adhered solids. It was apparent under magnification that in addition to the generalized attack and crevice-like attack that was observed visually, a number of micropits were also present in the region beneath the deposits. These micropits can most easily be observed in the profile map as the circular, green regions, indicating a depth of approximately 57 μm (2.24 mils) around the periphery of the features. However, the black center of many of these features indicated depths in excess of 10 μm (0.4 mils). The diameter of the largest pit appears to be approximately 900 μm (35.4 mils), which would give a diameter to depth ratio of approximately 16. The ratio indicates that these pits are broad and shallow, typical of pits on carbon steel. Additionally, a second micropit appears to be growing next to the deepest pit and coalescing with the larger pit. The coalescing forms areas of localized general attack, which is also typical of pitting on carbon steel.

Figure 5-14: LCM profile map (top) and depth profile (bottom) of area of attack beneath loosely adherent deposits during test exposed to compressed sludge.

A second micropit profile is shown in Figure 5-15. The depth profile conducted for this area covers only a single micropit to better characterize the pit itself. In this case, the pit penetrated to a depth of approximately 18 μm (0.7 mils) and has a diameter of roughly 400 μm (15.7 mils). The diameter to depth ratio is approximately 22, which is also typical of broad and shallow attack on carbon steel.

Figure 5-15: Optical image (top) and depth profile (bottom) of a single micropit beneath loosely adherent deposits during test exposed to compressed sludge.

While micropits were present throughout the areas covered by loosely adhered deposits, this was not the case for the entirety of the exposed surface. Areas of the surface where solids did not adhere did not have

any detectable localized corrosion, as seen in Figure 5-16. On the profile map (top right), no green, blue, are black areas are present, indicating that no localized or general attack in excess of 2 μm was present. Examination of the depth profile (bottom) reinforced that no corrosion features were present across the line scan conducted. The only feature that can be observed is the periodic oscillations in depth (approximately ± 1 μm) that are associated with the grinding of the sample surface to 600-grit.
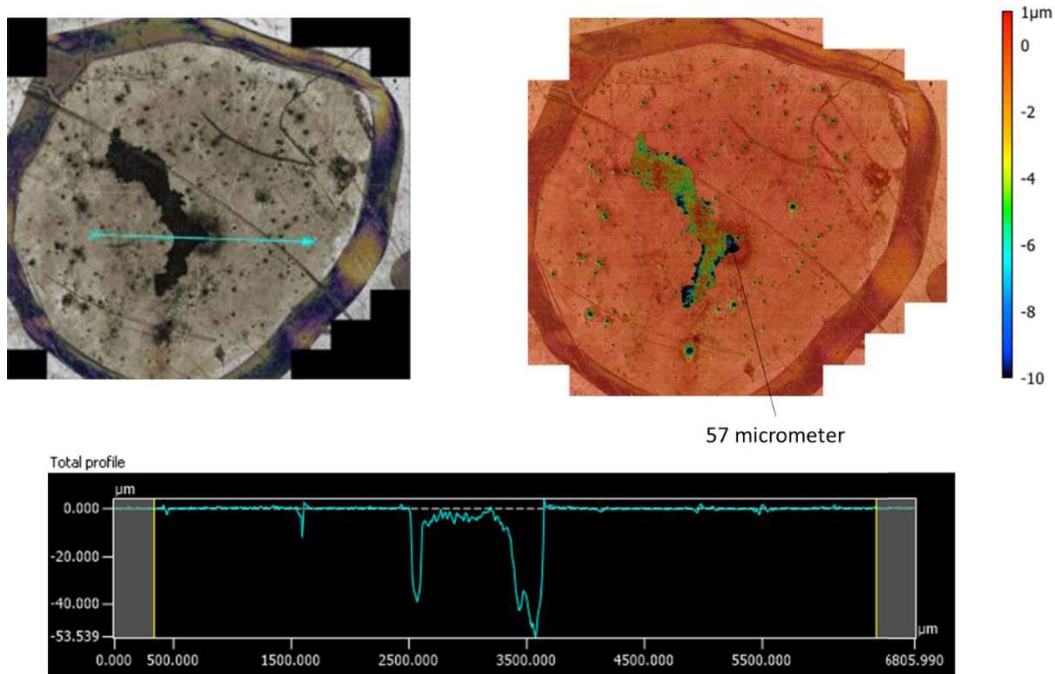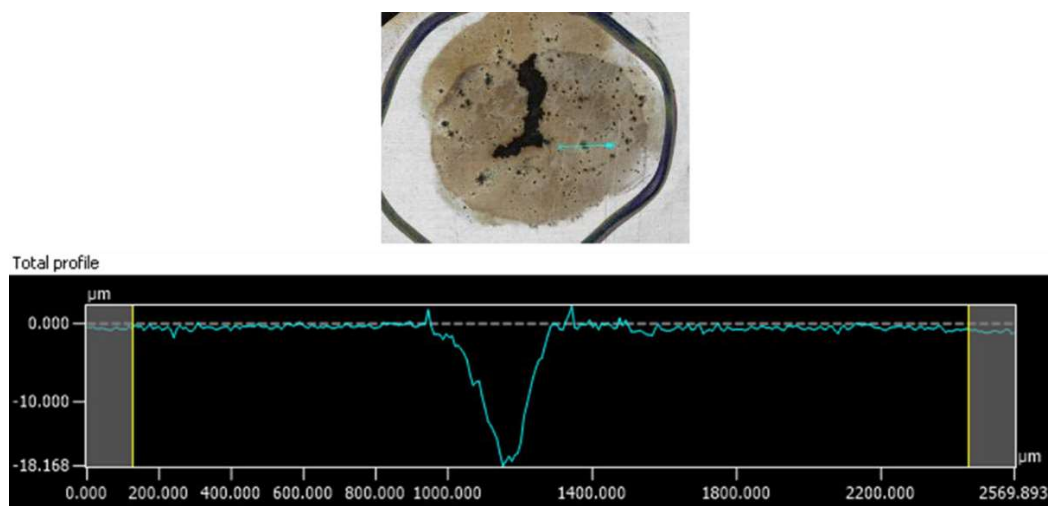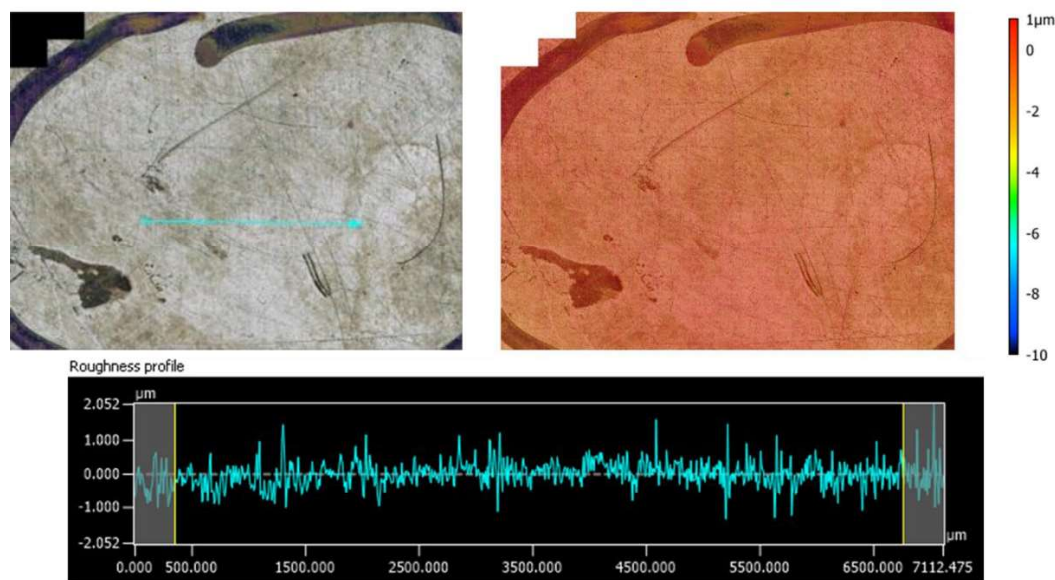

Figure 5-16: LCM profile map (top) and depth profile (bottom) of area away from loosely adherent deposits during test exposed to compressed sludge.

5.2 Secondary Liner Corrosion

5.2.1 Dissolved Oxygen Concentration Data

The dissolved oxygen (DO) concentration data, just before adding nitrogen and after the addition in the experimental vessel and in water trap, are presented in Figure 5-17. The DO values are close to 9 ppm before the addition of nitrogen, and close to zero after the addition. The time lag between the start of the nitrogen addition and DO values reaching zero was negligible. As seen in Figure 5-17, the GW simulant temperature remained close to 45 °C throughout the experimental duration. The gas phase oxygen concentration data is presented in Figure 5-18. As seen in the figure, the gas phase oxygen concentration quickly reached zero after addition of nitrogen.
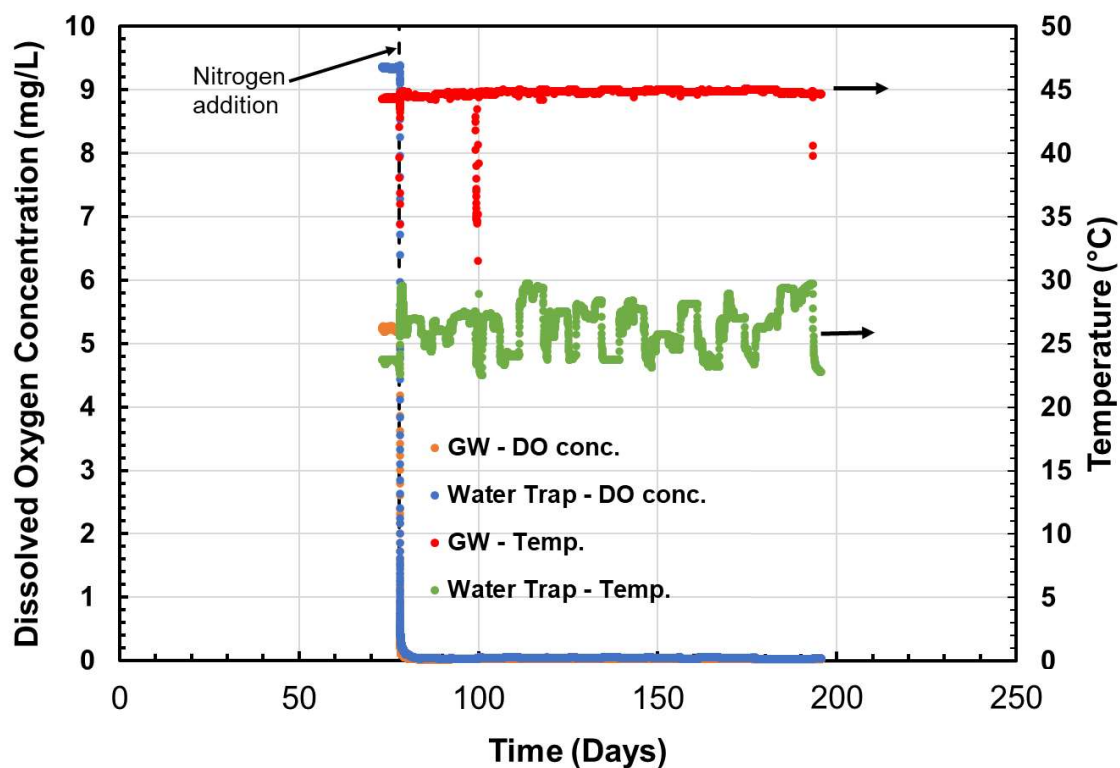
Figure 5-17: Liquid phase dissolved oxygen concentrations and temperatures versus time.
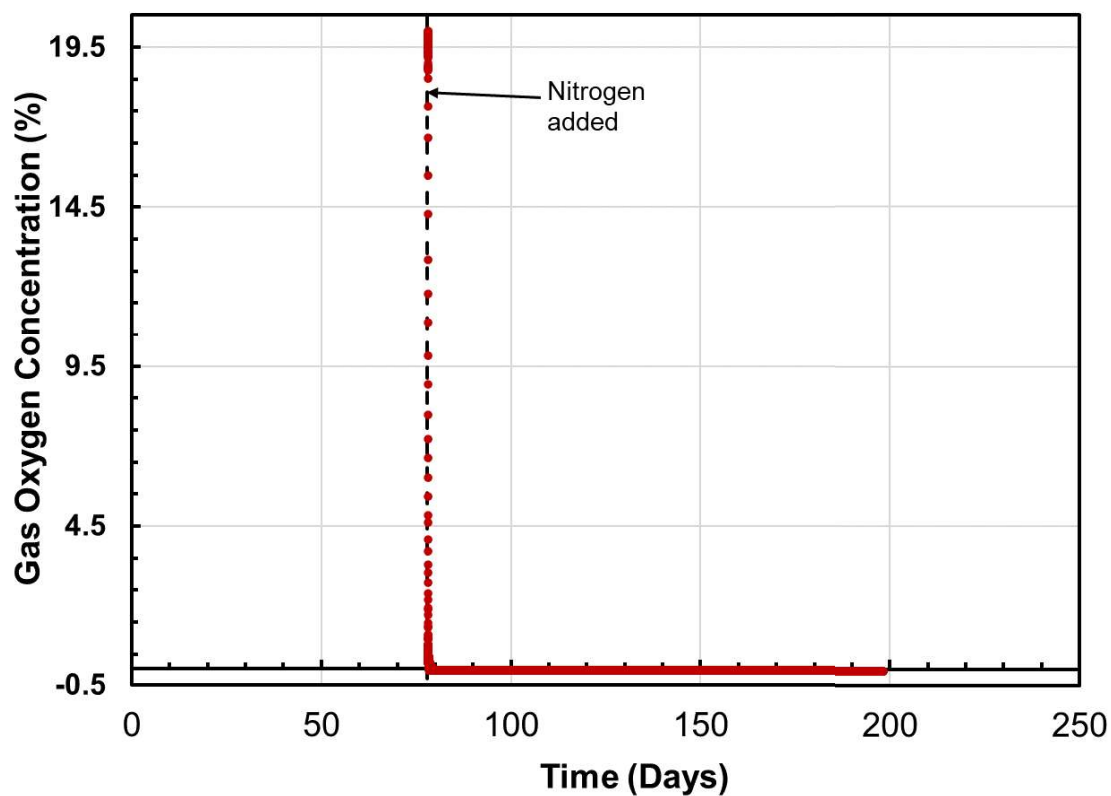
Figure 5-18: Gas phase dissolved oxygen concentrations versus time.

5.2.2 Coupon and ER Probe Data

Post-test images of the coupons are presented in Figure 5-19. Pitting and patch-like corrosion occurred on all the coupons. Images of the coupons sequentially exposed to GW only for 78 days and GW + N_2 for 120 days are presented in Figure 5-19 (a), and images of the coupons exposed to GW + N_2 continuously for 120 days are presented in Figure 5-19 (b). As seen in the figures, the coupons sequentially exposed to GW only for 78 days and then followed by GW + N_2 for 120 days accumulated significantly more corrosion products compared to the coupons exposed to GW+N_2 continuously for 120 days.

The ER probe data were collected using the cylindrical probe elements located at Levels 1 and 2 and immersed in the solution. The probes' data and the derived corrosion rates are presented in Figure 5-20 for the immersed, Level 1 and Level 2 probes. As seen in the figure, the corrosion rates decreased significantly after the nitrogen purge was initiated.

Level 3

Level 3

Level 2

Level 2

Level 1

Level 1
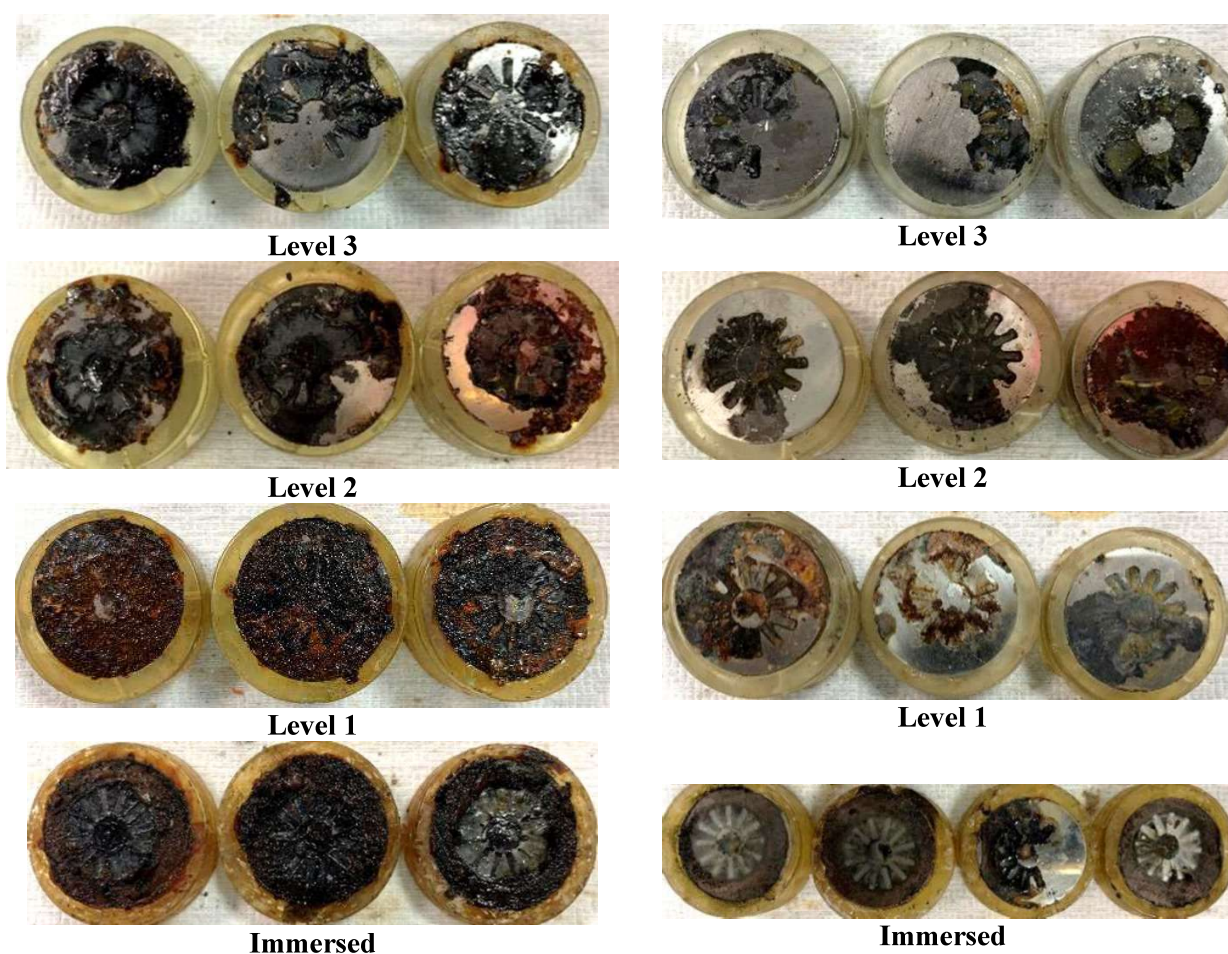
Immersed

Immersed

(a) Exposed to GW only for 78 days and GW + N_2 for 120 days

(b) Exposed to GW + N_2 for 120 days

Figure 5-19: Images of the coupons exposed to (a) GW only for 78 days and GW +N_2 for 120 days, and (b) GW + N_2 for 120 days.
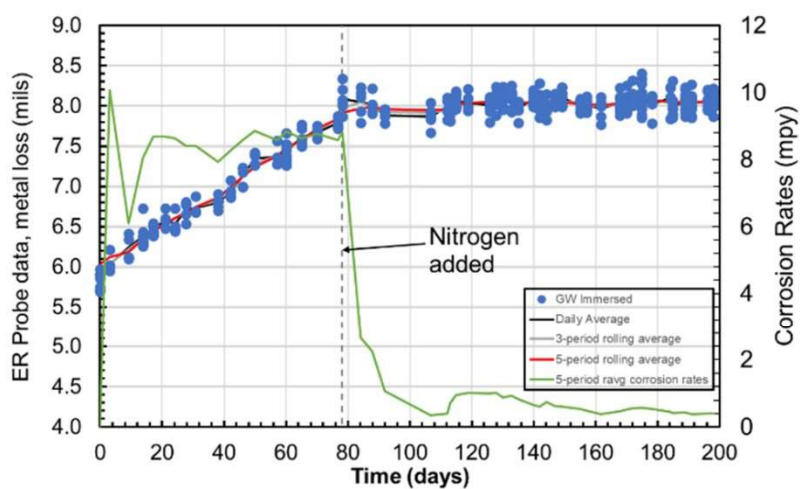
(a) Immersed
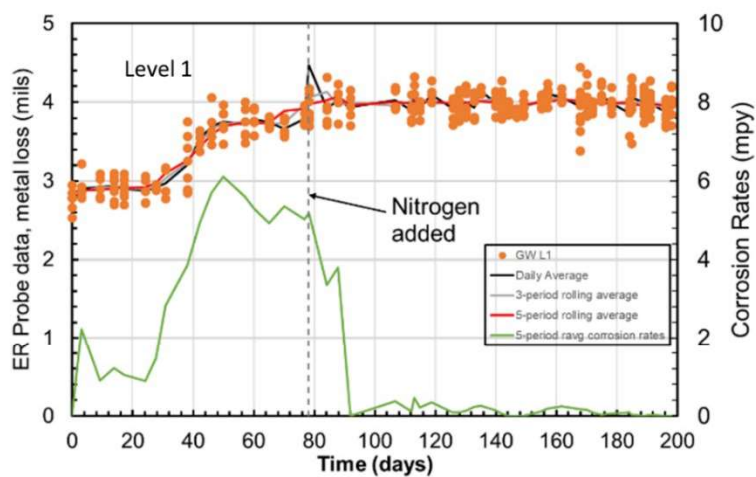
(b) Level 1

(c) Level 2

Figure 5-20: Electrical resistance data and corresponding corrosion rates for the probes located in (a) immersed, (b) Level 1, and (c) Level 2.

The corrosion rate data of the coupons sequentially exposed to GW for 78 days and GW + N$_2$ for 120 days are listed in Table 5-9. The average corrosion rates for coupons 1-3 for both the surface average and the deepest pit are shown in the last two columns of the table. These averages, along with their standard deviations are further illustrated in Figure 5-21. The corrosion rate data of the coupons exposed to GW + N$_2$ continuously for 120 days are listed in Table 5-10. The average corrosion rates for coupons 1-3 (or 4 for immersed) are shown in the last two columns of the table. These averages, along with their standard deviations are further illustrated in Figure 5-22. The surface average corrosion rates as a result of pre-corroding the sample for 78 days prior to exposing the coupon to N$_2$ for 120 days are an order of magnitude higher than the same rates for samples that were only exposed to the GW + N$_2$ continuously for 120 days. For the same comparison,the deepest pit corrosion rates are approximately lower by a factor of three. The corrosion rate data in Figure 5-21 and Figure 5-22 clearly show that the corrosion rates are significantly reduced in the presence of nitrogen, and nitrogen purging could be an effective corrosion mitigation strategy.
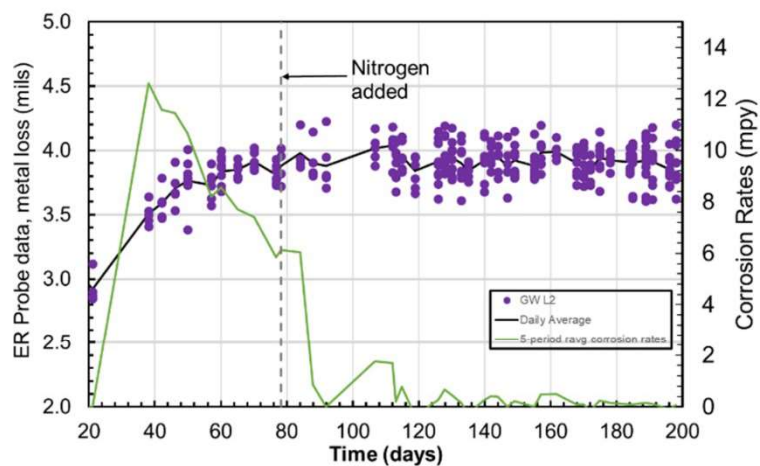
Table 5-9: Corrosion Rates of the Coupons Exposed to GW for 78 days and GW+N$_2$ for 120 days

Level	Corrosion Type	Corrosion Rate (mpy)			Average + Std of Surface Average Corrosion Rate (mpy)	Average + Std of Deepest Pit Corrosion Rate (mpy)
		Coupon 1	Coupon 2	Coupon 3		
Level 3	Surface Average	1.23	0.99	0.83	1.02 ± 0.20	12.1 ± 5.1
	Deepest Pit Corrosion	9.2	18.1	9.1		
Level 2	Surface Average	1.72	1.49	1.90	1.70 ± 0.20	15.0 ± 3.3
	Deepest Pit Corrosion	18.4	11.8	14.7		
Level 1	Surface Average	1.27	1.64	1.78	1.27 ± 0.26	15.3 ± 6.5
	Deepest Pit Corrosion	22.5	13.3	10.0		
Immersed	Surface Average	2.75	2.46	3.37	2.86 ± 0.46	15.6 ± 3.3
	Deepest Pit Corrosion	12.7	14.7	19.2		

Table 5-10: Corrosion Rates of the Coupons Exposed to GW+N$_2$ for 120 days

| Level | Corrosion Type | Corrosion Rate (mpy) | | | | Average + Std of Surface Average Corrosion Rate (mpy) | Average + Std of Deepest Pit Corrosion Rate (mpy) |
		Coupon 1	Coupon 2	Coupon 3	Coupon 4		
Level 3	Surface Average	0.30	0.60	0.45	–	0.45 ± 0.15	5.9 ± 0.9
	Deepest Pit Corrosion	4.9	6.2	6.7	–		
Level 2	Surface Average	0.38	0.26	0.42	–	0.35 ± 0.08	5.6 ± 0.6
	Deepest Pit Corrosion	6.0	5.6	5.0	–		
Level 1	Surface Average	0.37	0.17	0.42	–	0.32 ± 0.13	6.7 ± 2.0
	Deepest Pit Corrosion	7.7	8.1	4.4	–		
Immersed	Surface Average	0.32	0.27	0.34	0.42	0.33 ± 0.06	3.7 ± 1.5
	Deepest Pit Corrosion	2.3	2.6	4.9	5.1		
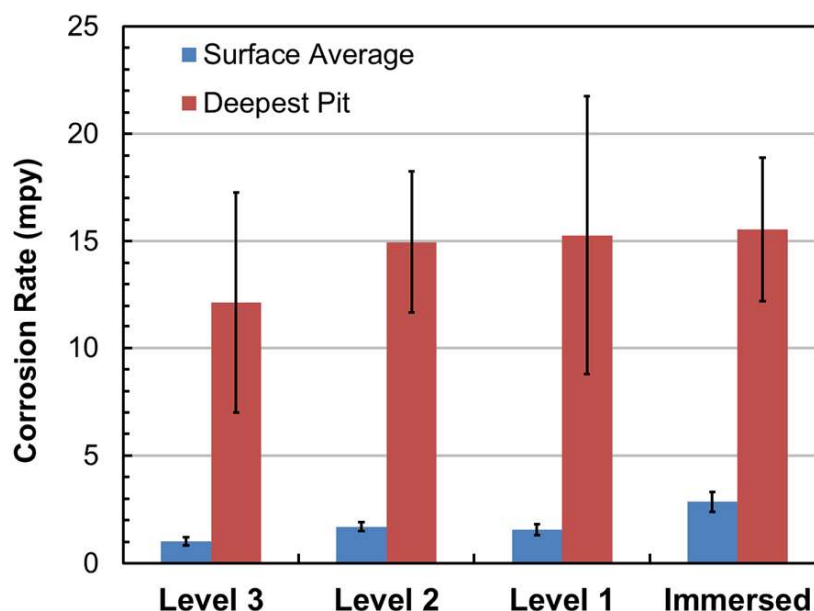
Figure 5-21: Surface average and deepest pit corrosion rates of the coupons sequentially exposed to GW for 78 days and GW + N$_2$ for 120 days. The standard deviations of the corrosion rates are represented by a solid black line in each bar.
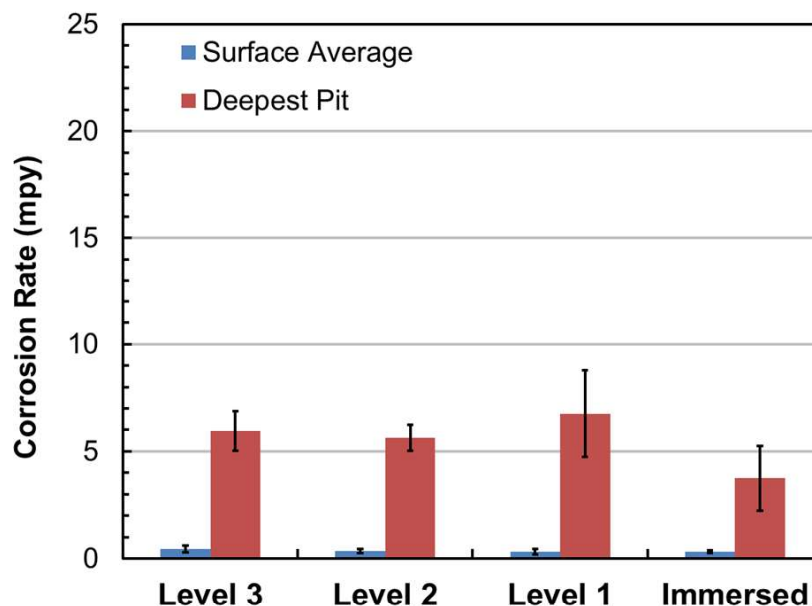
Figure 5-22: Surface average and deepest pit corrosion rates of the coupons exposed to GW + N₂ for 120 days. The standard deviations of the corrosion rates are represented by a solid black line in each bar.

The profiled images of the coupons exposed to GW for 78 days and GW + N₂ for 120 days are presented in Figure 5-23. Similarly, profiled images of the coupons exposed to GW + N₂ continuously for 120 days are presented in Figure 5-24. A comparison of the profiled images clearly shows that the coupons exposed to GW + N₂ continuously for 120 days corroded far less compared to the coupons exposed to GW for 78 days and GW + N₂ continuoulsy for 120 days The pit depths on the GW + N₂ for 120 days coupons typically ranged between 19 to 68 μm; the deepest pit depth on the majority of the coupons ranged between 35 to 55 μm; these smaller-depth pits could have formed when the coupons were initially placed in the vessel as the initial corrosion rates are generally higher than the long-term corrosion rates on carbon steel.
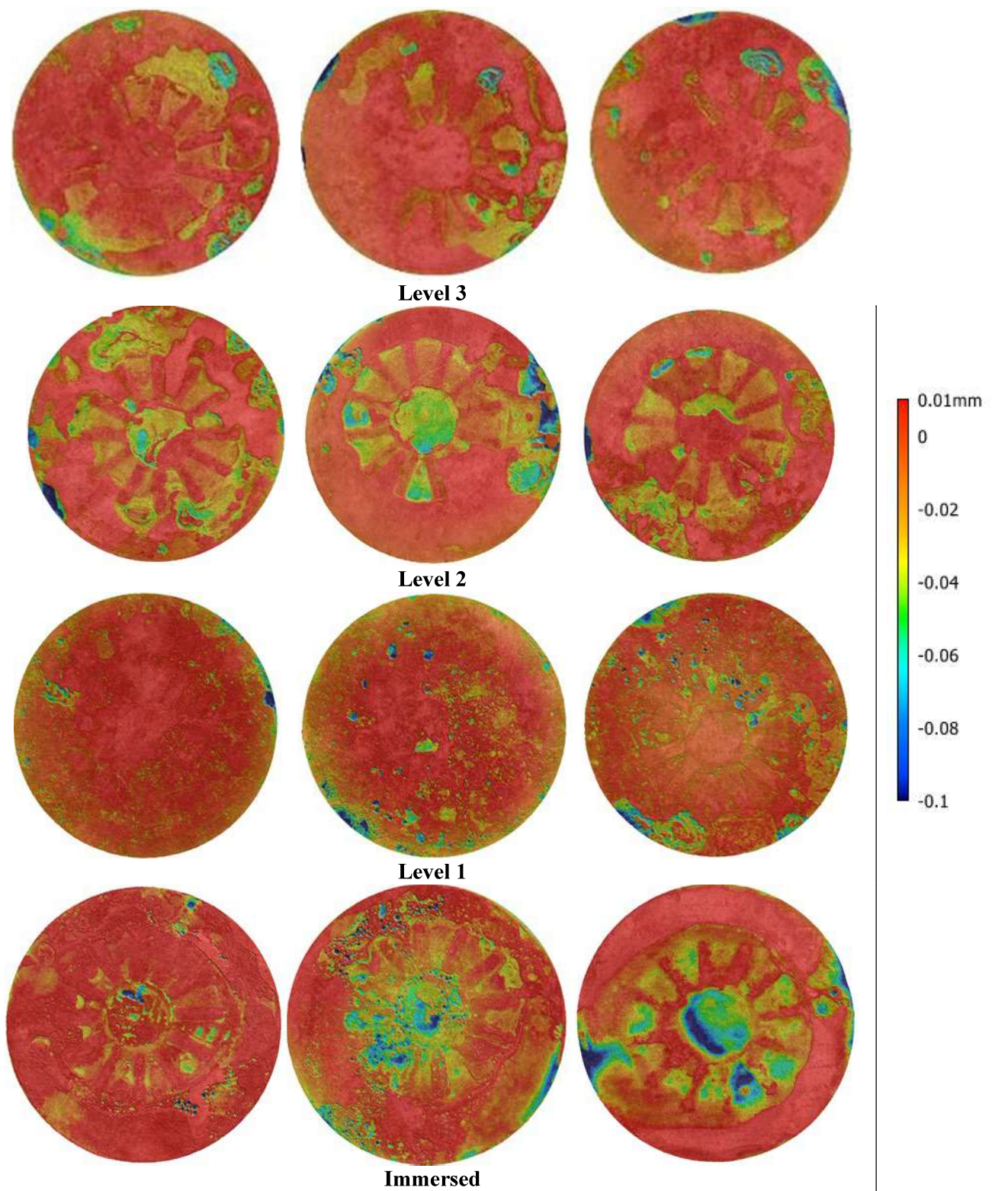
Figure 5-23: Profiled images of the coupons sequentially exposed to GW for 78 days and GW +N$_2$ for 120 days.

Figure 5-24: Profiled images of the coupons sequentially exposed to GW +N$_2$ for 120 days.

5.2.3 Comparison of Nitrogen with Vapor Corrosion Inhibitors

The corrosion rates of the coupons exposed to GW + N$_2$ are compared with the corrosion rates of the coupons that were exposed to GW + 100% VCI-B during testing in FY21 [15]. The tests with the vapor corrosion inhibitor (VCI) were performed in the same equipment, conditions and with the same type of samples as the tests 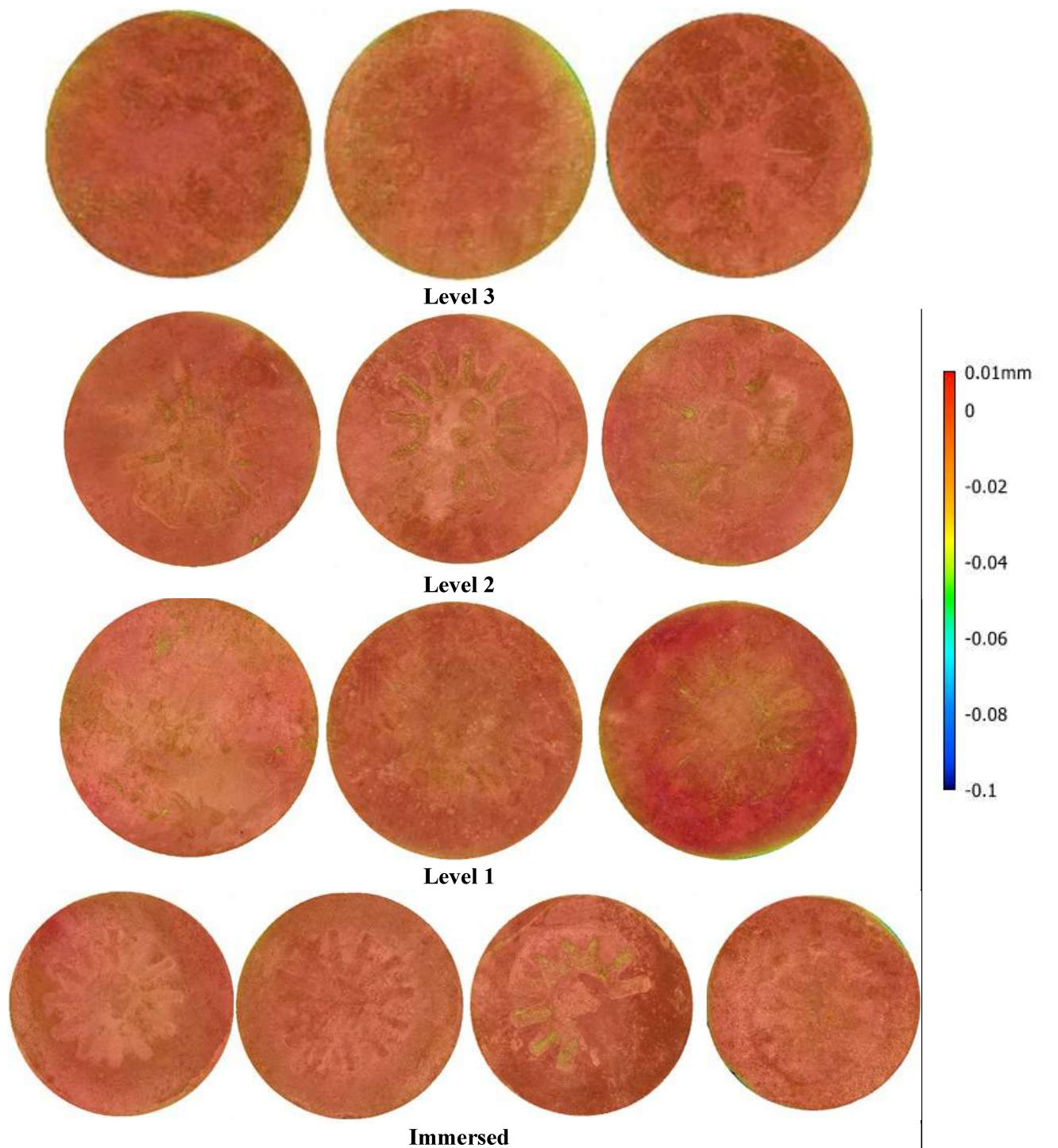that were performed with nitrogen. The comparison is shown in Table 5-11. The averages of the surface average corrosion rates for the coupons in immersed and Level 1 are less than 0.5 mpy for both the exposure conditions. The deepest pit corrosion rates of the coupons exposed to the two electrolytes conditions are also similar. This comparison is not completely accurate as the exposure times are different for the two environments. From this, it cannot be determined as to whether an additional 60 days of exposure to nitrogen will demonstrate a lower corrosion rate than the VCI. A complete comparison could be made by performing the tests with nitrogen for 180 days. Nevertheless, the results do indicate that both nitrogen and the VCI are effective corrosion inhibitors, for their given exposure times, if they are maintained at effective concentration levels.

The corrosion rates of the coupons exposed to GW for 78 days and GW + N$_2$ for 120 days are compared with the corrosion rates of the coupons that were exposed to GW for 60 days and GW + 100% VCI-B for 120 days, and GW for 60 days and GW + 50% VCI-B for 120 days. As shown in Table 5-12, the surface average corrosion rates at a given level for the three exposure conditions overlapped, showing that the coupons underwent a similar level of corrosion under the three exposure conditions. Similarly, the deepest pit corrosion rates at Levels 1 through 3 overlap with each other. The deepest pit corrosion rates of the coupons immersed in GW for 78 days and GW + N$_2$ for 120 days and that for GW for 60 days and GW + 50% VCI-B for 120 days also overlap. This comparison further highlights that the corrosion mitigation performance of nitrogen is comparable to the effective concentrations of the VCI-B.

Table 5-11: Corrosion Rates of the Coupons Exposed to GW+N$_2$ for 120 days and to GW + 100% VCI-B for 180 days

Level	Coupons Exposed to GW + N$_2$ for 120 days		Coupons Exposed to GW + 100% VCI-B for 180 days	
	Surface Average Corrosion Rate + Standard Deviation (mpy)	Deepest Pit Corrosion Rate + Standard Deviation (mpy)	Surface Average Corrosion Rate + Standard Deviation (mpy)	Deepest Pit Corrosion Rate + Standard Deviation (mpy)
Level 1	0.32 ± 0.13	6.7 ± 2.0	0.34 ± 0.34	8.0 ± 0.7
Immersed	0.33 ± 0.06	3.7 ± 1.5	0.17 ± 0.03	1.2 ± 0.2

Table 5-12: Corrosion Rates of the Coupons Sequentially Exposed to GW for 78 days and GW+N₂ for 120 days, GW for 60 days and GW + 100% VCI-B for 120 days, and GW for 60 days and GW + 50% VCI-B for 120 days.

Level	Coupons Exposed to GW and GW + N₂		Coupons Exposed to GW and GW + 100% VCI-B		Coupons Exposed to GW and GW + 50% VCI-B	
	Surface Average Corrosion Rate + Standard Deviation (mpy)	Deepest Pit Corrosion Rate + Standard Deviation (mpy)	Surface Average Corrosion Rate + Standard Deviation (mpy)	Deepest Pit Corrosion Rate + Standard Deviation (mpy)	Surface Average Corrosion Rate + Standard Deviation (mpy)	Deepest Pit Corrosion Rate + Standard Deviation (mpy)
Level 3	1.0 ± 0.2	12.1 ± 5.1	1.4 ± 0.1	13 ± 5.0	1.8 ± 1.4	10.5 ± 1.2
Level 2	1.7 ± 0.2	15.0 ± 3.3	1.9 ± 0.3	14 ± 3.0	1.7 ± 1.0	8.5 ± 0.6
Level 1	1.3 ± 0.3	15.3 ± 6.5	1.6 ± 0.3	11 ± 2.5	1.0 ± 0.1	14 ± 1.5
Immersed	2.9 ± 0.5	15.6 ± 3.3	3.1 ± 0.2	6.3 ±0.4	2.0 ± 0.2	20 ± 8

6.0 Conclusions

Observations and onclusions for activities that were performed for FY22 are summarized below.

6.1 Underdeposit Corrosion Testing

The following observations and conclusions were made from the long-term tests:

• All coupons embedded in the solids layer exhibited a similar low general corrosion rate (1-2 mpy). Additionally, the maximum pit depths measured were typically on the order of 2-5 mils. These results indicate that the environment beneath the solids is well inhibited. Given the similarity in the corrosion behavior, there is no indication that pitting increased with water content in the sludge.
• No aggressive attack was observed beneath a crevice former that was attached to the metal coupon and embedded within the solids layer. This indicates that the interstitial liquid had sufficient inhibitor to prevent crevice corrosion.
• The pits (i.e., termed micropits) measured on the coupons were much smaller in these FY22 tests than have been observed historically in uninhibited solutions. This suggests that pits may have initiated, but percolation of the inhibited interstitial liquid to the coupon surface may have repassivated the surface during the four-month test.

The following conclusions were drawn from the observations of the short-term electrochemical tests:

• The presence of the wet sludge resulted in an active shift in the negative direction of approximately 40 − 70 mV in the open circuit potential of the carbon steel coupon as compared to the interstitial liquid . It was also noted that compression of the sludge resulted in a decrease in the open circuit

56

potential of $10 - 20$ mV compared to that of the uncompressed sludge. The shift to more active potentials may be indicative of the initiation of localized or general corrosion beneath the solids.

•

• The corrosion rates measured by LPR for the interstitial liquid, the loose, wet sludge, and the compressed wet sludge were all less than 1 mpy. These rates are similar to what was observed in the long-term test and are indicative of a well inhibited environment. These corrosion rates were also corroborated by EIS measurements.

• CPP measurements in loose, wet sludge, and compressed wet sludge indicated that pitting may have initiated in the environment, but the pits were ultimately repassivated well before the completion of the test. Thus, sustainable, propagating pit are unlikely in this environment.

• Pit morphology characterization on a post-test CPP coupon indicated that the pits that formed were small. However, they tended to be broad and shallow and coalesce with neighboring pits. Thus, these pits had a morphology characteristic of carbon steel corrosion.

6.2 Secondary Liner Corrosion

The effectiveness of a nitrogen blanket for mitigating corrosion of the Hanford DSTs was investigated. The laboratory testing data showed the surface average corrosion rates decreased by an order of magnitude in the presence of nitrogen when compared with aerated conditions. These test results were compared with similar tests that were performed with a VCI. Although a complete comparison could not be made at this time due to differences in the exposure time, the results suggest that both effectively mitigate corrosion. A more complete comparison could be made by performing the nitrogen test for 180 days. In addition, the nitrogen and VCI-B comparison also showed that similar level of corrosion inhibition is achieved when weathered coupons were exposed to nitrogen, 100% VCI-B and 50% VCI-B.

6.3 Recommendations for FY23 Testing

Recommendations for follow-on work are summarized below. These recommendations will be incorporated into a proposal for FY23 activities.

Underdeposit Corrosion

➢ Investigate underdeposit corrosion under the non-porous adherent deposits with a more aggressive interstitial liquid composition (i.e., PF $\leq$ 1.2).

➢ Investigate the possibility of concentration cell corrosion (or cathodic polarization) beneath the sludge solids. The testing should address corrosion beneath adherent layers, the effect of concentration of the supernate above the wet, sludge layer, the effect of steel area exposed, and the effect of a temperature gradient between the supernate and the sludge solids.

Secondary Liner

➢ Investigate and determine the maximum oxygen concentration level such that corrosion is effectively mitigated. This test could be performed by varying the nitrogen blanket condition.

7.0 References

[1] "Double-Shell Tank Integrity Program", RPP-7574, Rev. 8.

[2] R. E. Fuentes, P. K. Shukla and B. J. Wiersma, "Task Technical and Quality Assurance Plan for Hanford Double Shell Waste Tank Corrosion Studies-FY21", SRNL-RP-2021-00178, Savannah River National Laboratory, Aiken, SC, March 2021.

[3] "Leak Inspection Report for Tank AY-102", RPP-RPT-60320.

[4] T. J. Barnes, K. D. Boomer, J. R. Gunter, and T. J. Venetz, "241-AZ Tank Farm Construction Extent of Condition Review for Tank Integrity", RPP-RPT-54818, August 1, 2013.

[5] "Double-Shell Tank Tertiary Leak Detection System Evaluation", RPP-RPT-55666, Rev. 3, 2016.

[6] RPP-RPT-58276, March 10, 2015, "Ultrasonic Inspection Results for Double-Shell Tank AP-102 – FY2015.

[7] R. E. Fuentes. B. J. Wiersma and K. Hicks, "Hanford Double Shell Waste Tank Corrosion Studies-Final Report FY14", SRNL-STI-2014-00616, Savannah River National Laboratory, Aiken, December 2014.

[8] R. E. Fuentes and R. B. Wyrwas, "Hanford Double Shell Waste Tank Corrosion Studies-Final Report FY15", SRNL-STI-2016-00117, Savannah River National Laboratory, Aiken, May 2016.

[9] R. E. Fuentes, "Hanford Double Shell Waste Tank Corrosion Studies-Final Report FY16", SRNL-STI-2016-00721, Savannah River National Laboratory, Aiken, February 2017.

[10] R. E. Fuentes, "Hanford Double Shell Waste Tank Corrosion Studies-Final Report FY17", SRNL-STI-2018-00116, Savannah River National Laboratory, Aiken, April 2018.

[11] R. E. Fuentes, P. K. Shukla, B. Peters, D. A. Hitchcock, "Hanford Double Shell Waste Tank Corrosion Studies-Final Report FY2018", SRNL-STI-2019-00014, Savannah River National Laboratory, Aiken, August 2019.

[12] R. E. Fuentes and P. K. Shukla, "Hanford Double Shell Waste Tank Corrosion Studies-Final Report FY2019", SRNL-STI-2020-00109, Savannah River National Laboratory, Aiken, July 2020.

[13] P. K. Shukla, et al., "Vapor Corrosion Inhibitors Effectiveness for Tank Bottom Plate Corrosion Control", PRCI, Inc. Report Catalog Number PR-015-153602-R01, 2018.

[14] P. K. Shukla, R. E. Fuentes, B. J. Wiersma, "Hanford Double Shell Waste Tank Corrosion Studies-Final Report FY2020", SRNL-STI-2021-00142, Savannah River National Laboratory, Aiken, July 2021.

[15] P.K. Shukla, R.E. Fuentes, and B. J. Wiersma, "Hanford Double Shell Waste Tank Corrosion Studies-Final Report FY2021", SRNL-STI-2022-00195, Savannah River National Laboratory, Aiken, August 2022.

[16] ASTM A515, "Standard Specification for Pressure Vessel Plates, Carbon Steel, for Intermediate- and Higher-Temperature Service", ASTM International, West Conshohocken, PA, 2003.

[17] RPP-RPT-42921, November 1999.

[18] Personal communication from L Stock, "AZ-101 Simulant June 3", June 2, 2020.

[19] R. E. Eibling, R. F. Schumacher, and E. K. Hansen, "Development of Simulants to Support Mixing Tests for High Level Waste and Low Activity Waste", WSRC-TR-2003-00220, December 2003.

[20] G. H. Beeman, "Composition of AZ-101 Envelope D and Associated Wastes, RPP-WTP-02-168, RPP-WTP-02-184, RPP-WTP-02-199, Battelle-Pacific Northwest Division, Richland WA 99352 (June 21, 2002), (July 31, 2002), (September 5, 2002).

[21] Private communication D. Lambert, M. Stone, and M. Siegfried on November 18, 2021.

[22] K. J. Cantrell, R. J. Serne, and G. V. Last, "Hanford Contaminant Distribution Coefficient Database and Users Guide", PNNL-13895, Rev. 1, June 2003.

[23] ASTM G59-97(2020), "Standard Test Method for Conducting Potentiodynamic Polarization Resistance Measurements", ASTM International, West Conshohocken, PA, 2020.

[24] NACE Corrosion Engineer's Reference Book, R. Baboian, editor, NACE International, Houston, TX, 2002.

[25] R. G. Kelley, "Electrochemical Techniques in Corrosion Engineering", University of Virginia, Center for Electrochemical Science and Engineering, 1992.

[26] ASTM G1-03 "Standard Practice for Preparing, Cleaning, and Evaluating Corrosion Test Specimens", ASTM International, West Conshohocken, PA, 2011.

[27] ASTM G5-13 "Standard Reference Test Method for Making Potentiodynamic Anodic Polarization Measurements", ASTM International, West Conshohocken, PA, 2013.

[28] T. Martin, "Outcomes from the August 2013 Expert Panel Oversight Committee Meeting,", RPP-ASMT-56781, Washington River Protection Solutions, LLC, Richland, WA, February 2014.

[29] P. E. Zapp, "Pitting Growth Rate in Carbon Steel Exposed to Simulated Radioactive Waste", WSRC-TR-96-0024, June 1996.

[30] "Standard Operating Procedure for Performing G192 Tests for WRPS Projects", SOP-052, August 2016.

Appendix A Chemical Composition of Simulants used in Secondary Liner Corrosion Testing

**Table A-1 Composition for GW simulant**

Temperature	45	°C
pH adjusted	7.6	
Volume	2	L

| Simulant Source	Formula	Concentration (M)	Weight required (g)
Sodium bicarbonate	$NaHCO_3$	1.750E-03	0.2940
Calcium hydroxide	$Ca(OH)_2$	1.500E-03	0.2223
Potassium nitrate	KNO_3	2.400E-04	0.0485
Ferric sulfate	$Fe_2(SO_4)_3$	6.250E-04	0.4999
Ferric chloride	$FeCl_3$	7.667E-05	0.0249
Strontium Nitrate	$Sr(NO_3)_2$	2.874E-06	0.0012
Sodium Metasilicate, 5-hydrate	$Na_2SiO_3.5H_2O$	6.000E-04	0.2546
Magnesium Chloride	$MgCl_2$	3.100E-04	0.0590
Acetic Acid	$C_2H_4O_2$	3.000E-04	0.0360

Appendix B Pictures of Secondary Liner Corrosion Testing Samples after Test
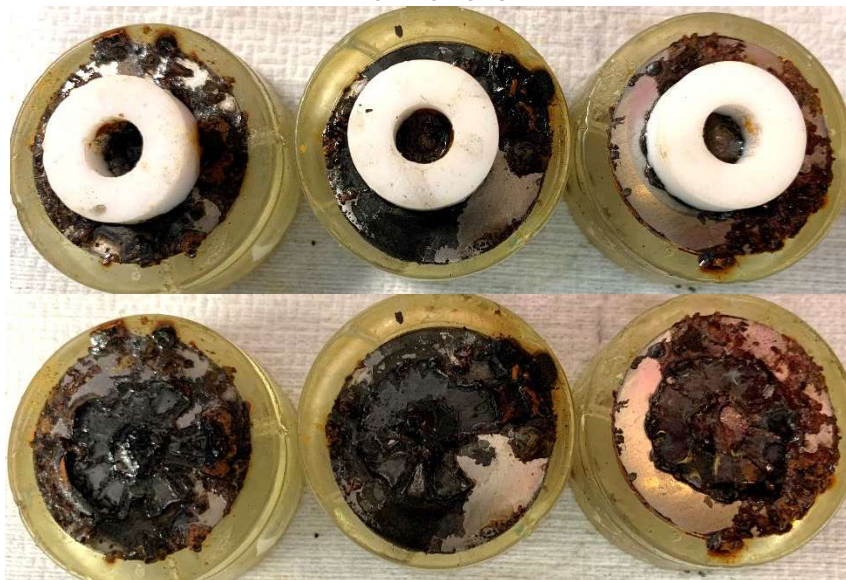
Samples cold mounted

Groundwater Coupons Test: Level 3
~6 months
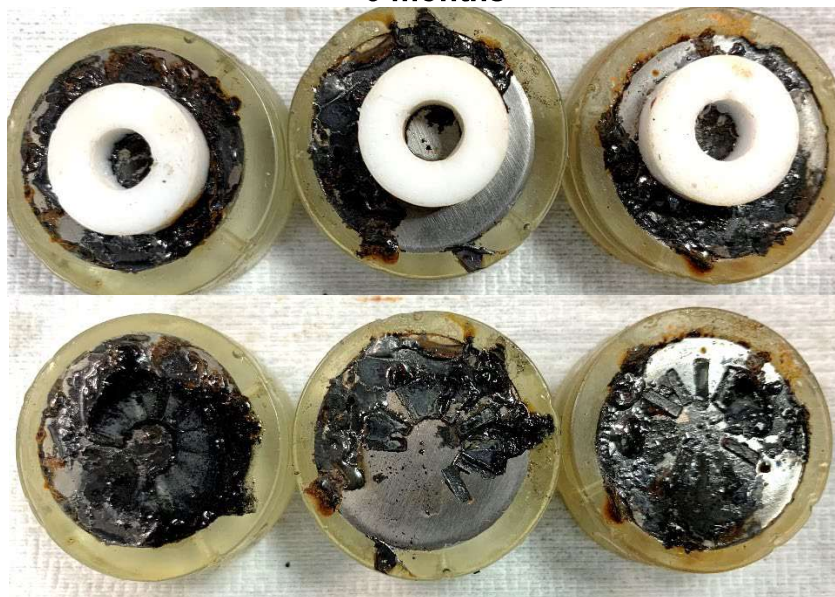
~4 months placed after nitrogen flow
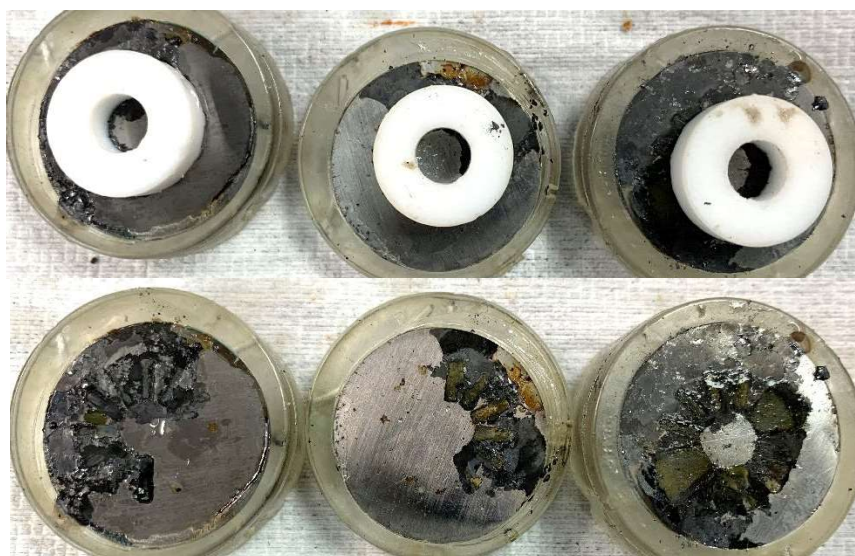
Groundwater Coupons Test: Level 2
~6 months

~4 months placed after nitrogen flow
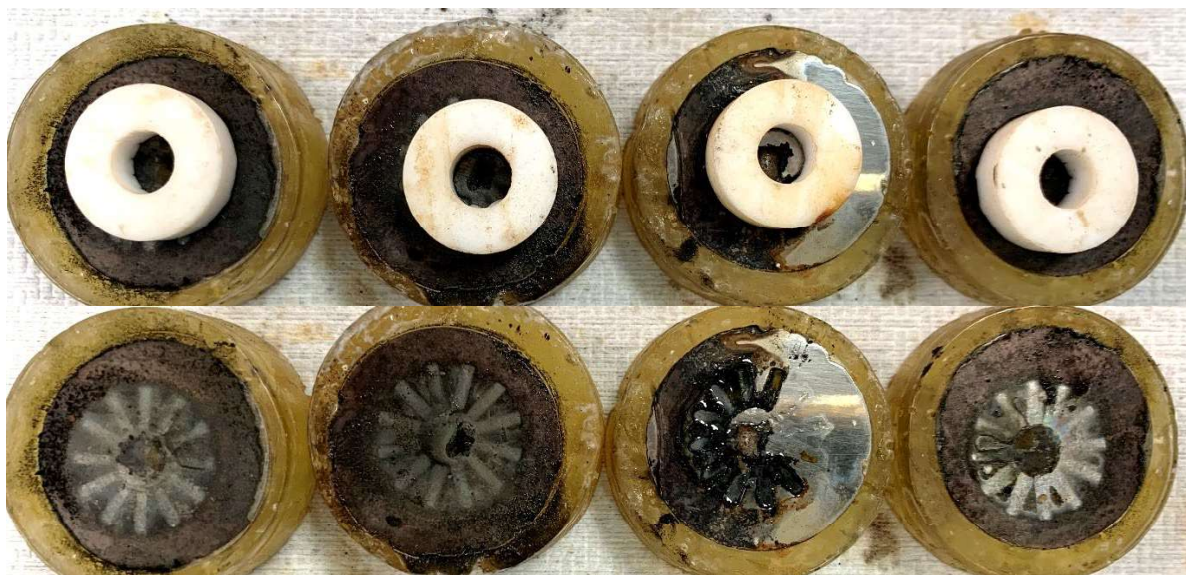
Groundwater Coupons Test: Level 1
~6 months

~4 months placed after nitrogen flow

Groundwater Test: Immersed
~6 months

~4 months placed after nitrogen flow

Distribution

alex.cozzi@srnl.doe.gov
joseph.manna@srnl.doe.gov
connie.herman@srnl.doe.gov
crystal_l_girardot@rl.gov
eric.skidmore@srnl.doe.gov
jason_s_page@rl.gov
Joshua.boerstler@srnl.doe.gov
michael.stone@srnl.doe.gov
Records Administration (EDWS)
Richard.wyrwas@srnl.doe.gov
robert_j_nelson@rl.gov
shawn_t_campbell@rl.gov
jason_r_gunter@rl.gov
kayle_d_boomer@rl.gov
pavan.shukla@srnl.doe.gov
roderick.fuentes@srnl.doe.gov